Astronomy
&
Astrophysics

Spectroscopic observations
of the candidate sgB[e]/X-ray binary CI Camelopardalis

R. I. Hynes[1,★], J. S. Clark[2], E. A. Barsukova[3], P. J. Callanan[4], P. A. Charles[1], A. Collier Cameron[5],
S. N. Fabrika[3], M. R. Garcia[6], C. A. Haswell[7,★★], Keith Horne[5], A. Miroshnichenko[8,9], I. Negueruela[10],
P. Reig[11,12], W. F. Welsh[13,★★], and D. K. Witherick[2]

[1] Department of Physics and Astronomy, University of Southampton, Southampton, SO17 1BJ, UK
[2] Department of Physics and Astronomy, University College London, Gower Street, London, WC1E 6BT, UK
[3] Special Astrophysical Observatory, Nizhnij Arkhyz, 369167, Russia
[4] University College, Department of Physics, Cork, Ireland
[5] School of Physics and Astronomy, University of St. Andrews, North Haugh, St. Andrews, Fife KY16 9SS, UK
[6] Harvard Smithsonian Center for Astrophysics, 60 Garden Street, Cambridge, MA 02138, USA
[7] Department of Physics and Astronomy, The Open University, Walton Hall, Milton Keynes, MK7 6AA, UK
[8] University of Toledo, Dept. of Physics and Astronomy, Toledo, OH 43606, USA
[9] Pulkovo Observatory, 196140 Saint-Petersburg, Russia
[10] Observatoire de Strasbourg, 11 rue de l'Université, 67000 Strasbourg, France
[11] Physics Department, University of Crete, PO Box 2208, 71003 Heraklion, Greece
[12] Foundation for Research and Technology–Hellas, 71110 Heraklion, Greece
[13] Dept. of Astronomy, San Diego State University, San Diego, CA 92182, USA

Abstract. We present a compilation of spectroscopic observations of the sgB[e] star CI Cam, the optical counterpart of XTE J0421+560. This includes data from before, during, and after its 1998 outburst, with quantitative results spanning 37 years. The object shows a rich emission line spectrum originating from circumstellar material, rendering it difficult to determine the nature of either star involved or the cause of the outburst. We collate all available pre-outburst data to determine the state of the system before this occurred and provide a baseline for comparison with outburst and post-outburst data. During the outburst all lines become stronger, and hydrogen and helium lines become significantly broader and asymmetric. After the outburst, spectral changes persist for at least three years, with Fe II and [N II] lines still a factor of ∼2 above the pre-outburst level and He I, He II, and N II lines suppressed by a factor of 2–10. We find that the spectral properties of CI Cam are similar to other sgB[e] stars and therefore suggest that the geometry of the circumstellar material is similar to that proposed for the other objects: a two component outflow, with a fast, hot, rarefied polar wind indistinguishable from that of a normal supergiant and a dense, cooler equatorial outflow with a much lower velocity. Based on a comparison of the properties of CI Cam with the other sgB[e] stars we suggest that CI Cam is among the hotter members of the class and is viewed nearly pole-on. The nature of the compact object and the mechanism for the outburst remain uncertain, although it is likely that the compact object is a black hole or neutron star, and that the outburst was precipitated by its passage through the equatorial material. We suggest that this prompted a burst of supercritical accretion resulting in ejection of much of the material, which was later seen as an expanding radio remnant. The enhanced outburst emission most likely originated either directly from this supercritical accretion, or from the interaction of the expanding remnant with the equatorial material, or from a combination of both mechanisms.

Key words. stars: individual: CI Cam – stars: emission line, B[e] – stars: radio emission stars: CI Cam – binaries: close

1. Introduction

On 1998 April 2 Smith et al. (1998) reported an *RXTE* All-Sky Monitor (ASM) detection of a bright, rapidly rising X-ray transient designated XTE J0421+560. Subsequently, Marshall et al. (1998) used the *RXTE* Proportional Counting Array (PCA) to refine the best fit position with an error circle of 1 arcmin radius. The bright ($V \sim 11$) B[e] star CI Cam (=MWC 84) was found to lie near to the centre of this error circle. Spectroscopic

Send offprint requests to: R. I. Hynes,
e-mail: rih@astro.as.utexas.edu
★ *Present address:* Department of Astronomy, The University of Texas at Austin, Austin, TX 78712, USA.
★★ Guest Observer, McDonald Observatory, University of Texas at Austin.

observations by Wagner et al. (1998) on 1998 April 3 revealed a rich emission line spectrum, similar to that reported by Downes (1984; see Sect. 2), but with the presence of He II emission features. These features had not been reported in previous spectra, and so by analogy to other X-ray binaries Wagner et al. (1998) proposed it to be the optical counterpart of XTE J0421+560. Photometric observations of the source at this time (e.g. Robinson et al. 1998; Garcia et al. 1998; Hynes et al. 1998) showed that CI Cam was some 2–3 mag brighter than had previously been reported.

Hjellming & Mioduszewski (1998a) reported the detection of a transient 19 mJy radio source at 1.4 GHz, corresponding to the optical position of CI Cam on 1998 April 1, thus confirming the identification of CI Cam as the optical counterpart. Subsequent observation of rapid radio variability established that the radio emission was of non-thermal (synchrotron) origin (Hjellming & Mioduszewski 1998b). Long term observations indicate that after the initial flare the radio emission underwent an unusually slow decay, with a 15 GHz flux of ~1.5 mJy about 40 months after the initial outburst (Pooley, priv. comm.). High spatial resolution maps obtained after the outburst indicated the presence of a clumpy ejection nebula (Mioduszewski et al., in preparation). These ejecta expand at ~1.0–1.5 mas d^{-1}, corresponding to an expansion velocity ~5000 km s^{-1} for a distance of 5 kpc.

Given the distance estimates (and optical luminosity implied) for CI Cam (e.g. $\log L/L_\odot \geq 4.86$; Clark et al. 2000; Robinson et al. 2002) it is clear that if it is a binary, as is likely, it is a high mass X-ray binary (HMXB). However CI Cam does not sit comfortably within the traditional divisions of HMXB mass donors into classical Be stars (~70 per cent) and OB supergiants (~30 per cent). While its luminosity suggests that it belongs to the later subset, such systems are typically short period binaries which accrete via Roche lobe overflow or direct wind fed accretion producing *persistent* X-ray emission (typically modulated at the orbital period). The presence of a rich emission line spectrum including forbidden lines, and a near IR excess due to hot dust (the observational criteria for the B[e] phenomenon; Allen & Swings 1976; Lamers et al. 1998) also mark a distinction from the other supergiant HMXB systems. Among the stars showing the B[e] phenomenon, the high luminosity of CI Cam makes it a Galactic counterpart to the Magellanic Cloud supergiant B[e] stars (sgB[e] stars) and we will refer to it as such for the rest of this work. CI Cam therefore appears to be the first bona fide sgB[e] star HMXB known, although direct evidence for binarity has proven elusive and a chance encounter of a compact object with the sgB[e] star although highly unlikely, cannot be ruled out.

This work presents a compilation of spectroscopy obtained before, during and after the 1998 outburst. A companion photometric compilation has been presented by Clark et al. (2000). Some of the outburst data included here has previously been presented by Barsukova et al. (1998) and Barsukova et al. (2002). In Sect. 2 we summarise the available pre-outburst data, including archival data with quantitative spectroscopy spanning ~30 years before the X-ray outburst and additional unpublished pre-outburst spectra. From these we identify the typical pre-outburst strengths of spectral lines and discuss their

stability. We then in Sect. 3 describe a series of new spectra running from a few days after the X-ray outburst to ~3 years later. In Sect. 4 we discuss extinction and distance estimates for the system and in Sect. 5 we review what is known about the mass donor star. Section 6 examines the changes in the continuum flux distribution and Sect. 7 the spectral lines and how these evolve through the outburst. Section 8 tests for the presence of shorter timescale variability. Finally in Sect. 9 we will discuss how all of these clues can help us build a picture of the nature of the system and the outburst mechanism and in Sect. 10 we summarise our conclusions.

2. Pre-outburst observations

Since CI Cam is bright and has a strong emission line spectrum, there exists a relatively large data set dating from 1933 to the present day. We present a summary of these observations, which include previously unpublished optical spectra from 1987 and 1994, to quantify an average "quiescent" state for CI Cam. Table 1 summarises the pre-outburst equivalent widths.

2.1. Published archival spectroscopy

The first observations of CI Cam were made by Merrill & Burwell (1933) and showed strong H I Balmer and weak Fe II emission. He I was seen to be strongly in emission but He II was absent. The first quantitative spectroscopic observations of CI Cam date from Chkhikvadze (1970). Spectra obtained during the period 1964–67 show strong H I and He I emission lines with no evidence of He II emission. Fe II lines were also in emission, the strongest being multiplets 27, 28, 37 and 38; there was no evidence for the Mg II 4481 Å line. Based on the strength of the Balmer emission lines Chkhikvadze (1970) suggested a spectral class of O6–B0 for CI Cam.

Allen & Swings (1976) describe further spectroscopic observations of CI Cam (although no date for the observations is provided). They note numerous emission lines of He I, Fe II and Si II. [N II] lines at 5755 and 6584 Å were present (the latter in the wings of the very strong Hα line); [O I] lines at 6300 and 6363 Å are possibly also detected. An estimate for the density of the circumstellar envelope of $N_e > 10^6$–10^7 cm^{-3} was derived from the strength of the [N II] lines. Higher excitation lines such as [O III] and [N III] appeared to be absent.

A 4000–7000 Å spectrum was obtained by Downes (1984) in 1984 January and once again was dominated by strong H I, He I and Fe II lines.

Miroshnichenko (1995) describes observations made between 1986 September and 1987 December. The spectrum was dominated by strong H I and He I lines, with numerous weak Fe II lines also present (as was C II emission at 4267 and 7234 Å). The H I Balmer lines were symmetrical and single peaked, with wings extending to ±250 km s^{-1} for Hα and Hβ.

Finally, Jaschek & Andrillat (2000) report observations from 1992 and 1998, the latter only two months before the outburst. 450 emission lines were observed, ~55 percent from Fe II, the remainder including H I, He I, O I, N I, Si II, Mg II, [O I], [N II], and [Fe II]. The Balmer lines show a very steep

Balmer decrement. O I 8446 Å is unusually strong, likely due to Lyβ fluorescence. Very few differences between the 1992 and 1998 epochs were seen. Since the latter spectra represent the highest quality pre-outburst spectra, as well as the closest to the X-ray outburst, we reanalysed them to establish a quantitative pre-outburst baseline.

2.2. Unpublished spectra taken at the Special Astrophysical Observatory

Three further unpublished observations of CI Cam were obtained by A. Miroshnichenko at the 6 m BTA telescope of the Special Astrophysical Observatory of the Russian Academy of Sciences (SAO RAS) on 1987 April 5 (~4460–5000 Å) and 1994 January 21 (~4000–4950 and ~5700–6800 Å).

The observations were made with a medium-resolution spectrograph SP-124 and a 1024-element one-dimensional photo-electric detector (Drabek et al. 1986). Data reduction was performed with the SIPRAN software developed at SAO RAS; no attempt at flux calibration was made. Due to the poor dynamic range of the scanner it was possible to obtain either profiles from the strong lines on an underexposed continuum, or a properly exposed continuum with saturated strong lines. Of the data presented here, the 1987 spectrum was exposed to search for weak lines, while the two spectra obtained in 1994 were obtained to determine the line profiles of the stronger emission lines. Consequently the continuum (and weaker lines) were poorly exposed for these spectra. We have chosen to include an equivalent width for the lines identified from the 5700–6700 Å spectrum, although we caution that the continuum level was uncertain in this spectrum.

2.3. Archival spectra from Haute-Provence

We obtained the 1998 spectra reported by Jaschek & Andrillat (2000) from the archive of the Observatoire de Haute-Provence (OHP). These spectra were obtained with the Aurelie spectrograph on the 1.52 m telescope using a Thomson array of 2026 photodiodes and a 300 line mm^{-1} grating, yielding a resolution of about 1.3 Å.

2.4. The "average" quiescent spectrum

We plot the pre-outburst optical spectrum (from 1998 OHP data) in Fig. 1a and in Table 1 we compile the equivalent widths of the strongest emission lines in quiescence. Coverage is clearly patchy, but no line exhibits dramatic variations in equivalent width. In particular the relative strengths of Balmer and He lines remain roughly the same. Downes (1984) does not include equivalent widths, but the relative line strengths plotted in his spectra (e.g. Hγ to He I 4471) look very similar to the results in Table 1, and also to Fig. 1a. It therefore appears that the pre-outburst spectrum was stable for at least ~30 years before the outburst, although large gaps in coverage are obviously present. As discussed in Sect. 7, the post-outburst spectrum is clearly different to this, but it remains to be seen whether the differences represent a delayed return to the pre-outburst quiescent state, or a new different quiescent state.

Table 1. Pre-outburst equivalent widths, in Å, of selected strong emission lines. Minus signs have been dropped for convenience as all lines are in emission. He I 4921 and 5015 Å have been omitted as these are unresolved from strong Fe II lines. Sources are [1] Chkhikvadze (1970), [2] Miroshnichenko (1995), [3] Sect. 2.2, [4] Jaschek & Andrillat (2000) and Sect. 2.3. Lines with no value given are not reported, outside the spectral range or too weak to reliably measure. Bracketed measurements were obtained from spectra with a poorly exposed continuum rendering the equivalent widths uncertain.

Line	1964–7[1]	1986–7[2]	1987[3]	1994[3]	1998[4]
Hδ 4100	4.9	–	–	5.1	–
Hγ 4340	13.4	10.5	–	10.9	10.5
Hβ 4861	53	65	57	44	46.5
Hα 6562	–	241	–	(397)	>300
He I 4026	4.0	–	–	3.6	–
He I 4471	10.6	–	–	10.7	9.6
He I 4713	9.3	–	8.0	8.8	8.0
He I 5875	93	–	–	(106.7)	73.6
He I 6678	–	–	–	(54.5)	53.2
He I 7065	–	–	–	–	89.4
He I 7281	–	–	–	–	34.0
[N II] 5755	–	–	–	–	3.5

3. Outburst and post-outburst observations

We next present a series of spectroscopic observations obtained during 1998 April and May, covering the outburst and immediate aftermath. Spectroscopy taken during this time indicates the presence of high excitation lines of He II at the time of the outburst which fade on a timescale ~10 days; similar variability is seen in most other lines observed during this period. Such behaviour occurs over longer timescales than the X-ray outburst; *XTE* observations reveal that the X-ray flux had already dropped by a factor of a hundred by April 4 (Belloni et al. 1999).

We obtained both blue and red spectra during the outburst, thus enabling us to follow the evolution of the outburst and determine changes in the circumstellar environment during this period. Spectra were obtained from four telescopes in the month following the X-ray outburst: the 1.5 m at the FLWO, the 6 m telescope of the SAO RAS, the 4.2 m WHT on La Palma and the McDonald Observatory 2.7 m. Subsequent observations obtained during the period between 1998 May and 2001 October constrain the long term post-outburst behaviour of the system. All of these observations are summarised in Table 2 and more details are given in the following subsections.

3.1. F. L. Whipple observatory observations

A series of spectra were obtained using the 1.5 m telescope at the F. L. Whipple Observatory (FLWO) and the FAST spectrometer. These observations began soon after the outburst was discovered and continued until the end of 1998. The spectra were obtained with two different gratings, of
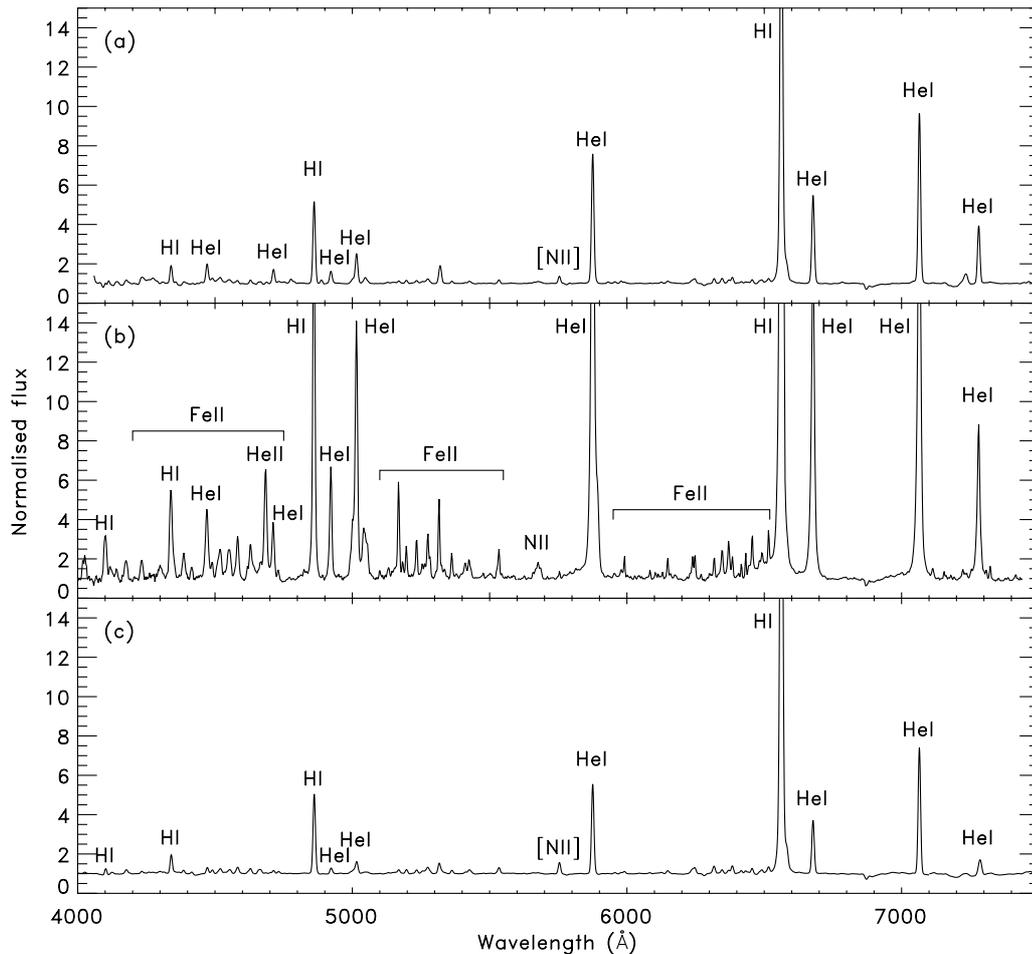
Fig. 1. Comparison between normalised spectra from **a)** before the outburst (1998 January 27–28), **b)** early in the outburst (1998 April 4), and **c)** after the outburst (2000 February 6 for $\lambda > 7100$ Å and 2000 December 1 elsewhere). Major features are labelled. The strongest groups of Fe II lines are also indicated, but other species are present in these complexes and Fe II lines are also found elsewhere.

300 and 1200 lines mm^{-1}, giving 3.0 and 1.1 Å resolution respectively.

These observations included a series of 370 2 s spectra with ~1.1 Å resolution and a dispersion of 0.4 Å pix^{-1}, covering 6040–7035 Å which were obtained on the night of 1998 April 2. We searched for shifts in the velocities of the emission lines by cross-correlating all the spectra against a single template. The largest shifts are ± 12 km s^{-1}, the rms in the velocities is 3.6 km s^{-1}. Given the high airmass (from 1.5 to 2.0) and the 2.0 arcsec slit, these variations are likely due to variable illumination of the slit rather than intrinsic motions in the emission lines, as the velocity resolution was about 50 km s^{-1}. Nonetheless, we searched for periodicities in the velocities using the algorithm of Stellingwerf (1978), but found nothing significant. We will further discuss evidence for variations in line strengths and profiles in Sect. 8.

3.2. Special Astrophysical Observatory observations

Outburst observations spanning 1998 April to May were made using the 6 m BTA telescope of the SAO RAS. A medium resolution spectrograph, SP–124 (at the Nasmyth–1 focus), was used with a Photometrix 1024 × 1024 CCD detector and the

B1 grating (600 lines mm^{-1}) providing a spectral dispersion of 2.4 Å pixel^{-1} in two overlapping spectral ranges 3700–6100 and 5000–7500 Å. The slit width employed was either 1 arcsec or 2 arcsec, depending on seeing conditions, providing a spectral resolution of ~4 Å or ~8 Å respectively. Primary reduction of the CCD spectra including corrections for the dark current, debiasing and sky subtraction was accomplished with MIDAS (1996 Nov. version). He–Ne–Ar lamps were used for wavelength calibration.

3.3. WHT/UES observations

CI Cam was observed at high resolution using the Utrecht Echelle Spectrograph (UES) on the William Herschel Telescope (WHT) on La Palma on 1998 April 9–11. Spectra were extracted using a simple (non-optimal) extraction with sky subtraction using ECHOMOP software. Cosmic rays were removed by hand.

3.4. McDonald observatory observations

Intermediate dispersion spectroscopy was obtained on the nights of 1998 April 18–20 using the Large Cassegrain

Table 2. Summary of spectroscopic observations, both pre-, during, and post-outburst which were quantitatively analysed for this work. In some cases multiple spectra from the same night covering the same wavelength range have been merged on one line; in this case start and end times refer to the first and last spectrum and do not indicate total exposure time. Continued on the next page.

Date	Telescope	UT Start	UT End	Number	Wavelength Range (Å)	Resolution (Å)
Pre-outburst						
05/04/87	SAO RAS 6-m	23:12	23:50	1	4460–5005	1.1
06/04/87	SAO RAS 6-m	00:20	00:45	1	6620–7290	2.1
21/01/94	SAO RAS 6-m	17:38	18:06	1	4000–4900	2.2
21/01/94	SAO RAS 6-m	18:15	18:28	1	5700–6700	2.1
26/01/98	OHP 1.52-m	21:37	22:20	1	4060–4930	1.3
27/01/98	OHP 1.52-m	21:16	22:46	1	4860–5730	1.3
27/01/98	OHP 1.52-m	23:14	00:44	1	6250–7110	1.3
28/01/98	OHP 1.52-m	01:04	02:34	1	4060–4930	1.3
28/01/98	OHP 1.52-m	23:02	00:32	1	8040–8900	1.3
29/01/98	OHP 1.52-m	01:08	02:38	1	5560–6430	1.3
29/01/98	OHP 1.52-m	03:00	04:30	1	7060–7930	1.3
Outburst						
03/04/98	FLWO 1.5-m	02:41	02:44	3	3580–7450	3.0
03/04/98	FLWO 1.5-m	02:47	04:19	370	6040–7035	1.1
04/04/98	SAO RAS 6-m	17:07	17:11	2	3700–6130	4.0
04/04/98	SAO RAS 6-m	17:14	17:15	1	4990–7460	4.0
05/04/98	SAO RAS 6-m	15:33	15:35	1	3700–6130	4.0
05/04/98	SAO RAS 6-m	15:40	15:41	1	4990–7460	4.0
06/04/98	SAO RAS 6-m	15:47	16:20	2	3700–6130	4.0
06/04/98	SAO RAS 6-m	15:52	16:04	3	4990–7460	4.0
09/04/98	WHT 4.2-m	21:15	21:46	2	3870–6110	0.1
10/04/98	WHT 4.2-m	20:50	21:48	3	3870–6110	0.1
11/04/98	WHT 4.2-m	20:49	21:51	5	3870–6110	0.1
18/04/98	McDonald 2.7-m	02:47	05:00	61	6190–6900	1.2
18/04/98	FLWO 1.5-m	03:08	03:28	11	3630–7490	3.0
19/04/98	McDonald 2.7-m	02:26	04:07	65	6190–6900	1.2
19/04/98	FLWO 1.5-m	02:54	03:10	2	3740–4740	1.1
19/04/98	FLWO 1.5-m	03:08	03:18	3	4310–5310	1.1
19/04/98	FLWO 1.5-m	03:27	03:32	4	6040–7030	1.1
20/04/98	McDonald 2.7-m	02:12	04:54	80	6190–6900	1.2
19/04/98	SAO RAS 6-m	14:58	15:15	25	3700–6130	8.0
19/04/98	SAO RAS 6-m	15:19	15:27	2	4990–7460	8.0

Spectrometer (LCS) on the McDonald Observatory 2.7 m telescope. Each night involved a series of observations spanning about 2 hours to search for variability; this will be discussed further in Sect. 8. Reduction and extraction were performed using standard `iraf` tasks. Observations of neon arc lines were performed at 20 min intervals to provide wavelength calibration. Corrections were made to the interpolated wavelength solution using night sky emission lines. As for the FLWO observations, no significant wavelength variations were found.

3.5. WHT/ISIS observations

Intermediate and high dispersion spectroscopy was obtained on several nights from 1998–2001 using the ISIS dual-beam spectrograph on the WHT. Most exposures used the blue arm with the EEV10 or EEV12 CCD. The second spectrum from 2001 April 28 used the red arm with the TEK4 CCD. Slit widths were 0.7–1.0 arcsec. Reduction and extraction were performed using standard `iraf` tasks. Copper-neon and/or copper-argon lamps were observed to provide wavelength calibration. No flux calibration of these spectra was attempted.

3.6. Loiano and Asiago observatory observations

Post-outburst spectra of the source were obtained in 1999 January 5 and 2000 February 6 using the 1.52 m G. D. Cassini telescope at the Loiano Observatory (Italy). The telescope was equipped with the Bologna Faint Object Spectrograph and Camera (BFOSC) and a 2048 × 2048 Loral CCD. In January 1999 grism #8 was used, giving a resolution of ~3 Å, and in February 2000 the low-dispersion grisms #3 (blue) and #4 (red) were used. One further spectrum was taken on 1998 November 1st using the 1.82 m telescope at Asiago Observatory (Italy), equipped with the Asiago Faint Object Spectrograph and Camera (AFOSC) and a 1024×1024 thinned SITe CCD. This instrument is identical to BFOSC and grism #8 was used, giving the same resolution.

Table 2. continued.

Date	Telescope	UT Start	UT End	Number	Wavelength Range (Å)	Resolution (Å)
Post-outburst						
16/05/98	SAO RAS 6-m	18:08	18:21	3	3700–6130	4.0
16/05/98	SAO RAS 6-m	18:29	18:40	2	4990–7460	4.0
20/07/98	WHT 4.2-m	05:43	06:01	4	3500–7000	3.1
21/07/98	WHT 4.2-m	05:57	06:06	2	4800–5200	0.4
15/09/98	FLWO 1.5-m	09:49	09:53	3	3660–7530	3.0
17/09/98	FLWO 1.5-m	10:46	10:50	2	3660–7530	3.0
18/09/98	FLWO 1.5-m	11:43	11:47	2	3660–7530	3.0
19/09/98	FLWO 1.5-m	11:42	11:44	3	3660–7530	3.0
21/09/98	FLWO 1.5-m	08:54	08:56	3	3660–7530	3.0
23/09/98	FLWO 1.5-m	11:42	11:46	2	3660–7530	3.0
24/09/98	FLWO 1.5-m	11:41	11:45	2	3660–7530	3.0
29/09/98	FLWO 1.5-m	11:57	11:58	3	3630–7490	3.0
30/09/98	FLWO 1.5-m	08:37	08:39	3	3660–7530	3.0
14/10/98	FLWO 1.5-m	10:19	10:22	2	3650–7520	3.0
15/10/98	FLWO 1.5-m	10:55	10:58	2	3650–7520	3.0
16/10/98	FLWO 1.5-m	10:44	10:47	2	3650–7520	3.0
23/10/98	FLWO 1.5-m	10:49	10:51	3	3580–7450	3.0
29/10/98	FLWO 1.5-m	09:03	09:07	2	3650–7520	3.0
01/11/98	Asiago 1.82-m	02:20	02:35	1	6360–8060	3.3
12/11/98	FLWO 1.5-m	10:02	10:13	3	3630–7500	3.0
13/11/98	FLWO 1.5-m	11:41	11:44	3	3630–7500	3.0
14/11/98	FLWO 1.5-m	10:02	10:06	3	3630–7500	3.0
15/11/98	FLWO 1.5-m	08:14	08:17	3	3630–7500	3.0
16/11/98	FLWO 1.5-m	10:41	10:44	3	3630–7500	3.0
17/11/98	FLWO 1.5-m	11:08	11:10	4	3630–7500	3.0
18/11/98	FLWO 1.5-m	09:06	09:18	4	3630–7500	3.0
19/11/98	FLWO 1.5-m	09:40	09:44	3	3660–7530	3.0
21/11/98	FLWO 1.5-m	09:31	09:34	3	3660–7530	3.0
22/11/98	FLWO 1.5-m	08:35	08:39	3	3660–7530	3.0
23/11/98	FLWO 1.5-m	09:04	09:07	3	3660–7530	3.0
24/11/98	FLWO 1.5-m	10:24	10:27	3	3660–7530	3.0
25/11/98	FLWO 1.5-m	07:56	08:01	3	3660–7530	3.0
26/11/98	FLWO 1.5-m	07:47	07:51	3	3660–7530	3.0
27/11/98	FLWO 1.5-m	08:23	08:27	3	3660–7530	3.0
30/11/98	FLWO 1.5-m	11:17	11:22	3	3660–7530	3.0

3.7. Haute Provence observations

Post-outburst spectra obtained from OHP in 1999 used the same configuration as the 1998 pre-outburst observations, hence the details are the same as described in Sect. 2.3.

3.8. Calar Alto observations

One low-resolution flux-calibrated spectrum was taken on 2000 January 29 using the blue arm of the TWIN spectrograph on the 3.5 m telescope at Calar Alto (Spain) and a 2000×800 thinned SITe CCD.

3.9. Skinakas Observatory observations

Spectra taken on 2001 July 19 & October 16 were taken with the 1.3 m f/7.7 Ritchey-Chretien telescope at Skinakas Observatory (Crete, Greece). This was equipped with a 2000×800 ISA SITe CCD and a 1302 lines mm^{-1} grating (using a 80 μm slit), giving a dispersion of $\sim$1 Å pixel^{-1}.

3.10. Steward observatory observations

Finally three spectra were obtained using the Bok 2.3 m telescope of the Steward Observatory with the Boller and Chivens long slit spectrograph and a 1200×800 CCD. A first order 1200 lines mm^{-1} grating was used and there were no filters. Flux calibration was not reliable as there were significant slit losses.

4. Interstellar extinction and distance estimates

There remain large uncertainties about the interstellar extinction to CI Cam, and even more so concerning the distance. A number of extinction estimates have been made but these are complicated by the uncertainty about how much of the measured extinction is intrinsic to the source; different methods

Table 2. continued.

Date	Telescope	UT Start	UT End	Number	Wavelength Range (Å)	Resolution (Å)
10/12/98	FLWO 1.5-m	05:59	06:03	3	3660–7530	3.0
12/12/98	FLWO 1.5-m	07:29	07:32	3	3660–7530	3.0
13/12/98	FLWO 1.5-m	05:29	05:33	3	3660–7530	3.0
14/12/98	FLWO 1.5-m	09:25	09:29	3	3660–7530	3.0
19/12/98	FLWO 1.5-m	06:07	06:11	3	3660–7530	3.0
20/12/98	FLWO 1.5-m	06:22	06:27	3	3660–7530	3.0
21/12/98	FLWO 1.5-m	07:35	07:39	3	3660–7530	3.0
22/12/98	FLWO 1.5-m	06:08	06:12	3	3660–7530	3.0
23/12/98	FLWO 1.5-m	06:11	06:15	3	3660–7530	3.0
25/12/98	FLWO 1.5-m	08:32	08:36	3	3660–7530	3.0
26/12/98	FLWO 1.5-m	04:52	04:56	3	3660–7530	3.0
27/12/98	FLWO 1.5-m	05:14	05:17	3	3660–7530	3.0
28/12/98	FLWO 1.5-m	03:14	03:18	3	3660–7530	3.0
03/01/99	OHP 1.52-m	00:26	01:55	1	8040–8900	1.3
03/01/99	OHP 1.52-m	03:30	05:30	1	4060–4930	1.3
03/01/99	OHP 1.52-m	20:05	21:35	1	4860–5730	1.3
03/01/99	OHP 1.52-m	22:11	23:41	1	5560–6430	1.3
04/01/99	OHP 1.52-m	00:04	01:34	1	6250–7110	1.3
04/01/99	OHP 1.52-m	02:33	04:33	1	7060–7930	1.3
05/01/99	Loiano 1.52-m	21:17	21:27	1	6360–8220	3.3
29/01/00	Calar Alto 3.5-m	23:44	23:49	1	3700–6800	6.1
06/02/00	Loiano 1.52-m	21:11	21:41	1	3500–5400	5.5
06/02/00	Loiano 1.52-m	20:33	21:06	2	3530–8830	8.3
19/07/00	Skinakas 1.3-m	02:30	02:35	1	5550–7550	4.5
16/10/00	Skinakas 1.3-m	01:37	01:40	1	5250–7300	4.5
01/12/00	WHT 4.2-m	20:22	20:37	3	3700–7200	3.6
01/12/00	WHT 4.2-m	21:06	21:37	3	3870–4310	0.3
28/04/01	WHT 4.2-m	20:53	21:03	1	3600–4030	0.3
28/04/01	WHT 4.2-m	20:45	21:03	15	6300–6700	0.6
08/08/01	Skinakas 1.3-m	01:42	01:47	1	5460–7430	4.5
13/09/01	Skinakas 1.3-m	00:45	00:48	1	5230–7200	4.5
23/10/01	Bok 2.3-m	10:30	10:46	3	3885–5030	1.8

may be more or less sensitive to this depending on what is actually measured. Consequently it is of value to compare as many independent methods as possible. We discuss only recent estimates as these are likely to use higher quality data and/or more sophisticated models, superseding earlier estimates (e.g. Chkhikvadze 1970).

A number of attempts have been made to fit the broad band optical–far IR spectral energy distribution (SED) using a model including extinction as a free parameter. Belloni et al. (1999) fitted the SED using a Kurucz atmosphere and a dust model and derived $E(B - V) = 1.18 \pm 0.04$ mag and hence $A_V \sim 4.4$ mag. Clark et al. (2000) used a similar model to derive $A_V \sim 3.71$ mag. Zorec (1998) used a model in which the interstellar extinction and distance were constrained to be consistent rather than independent, and estimated $d \sim 1.75$ kpc, $E(B - V)_{\rm ism} \sim 0.8$ mag and $A_{V,\rm local} \sim 2.4$ mag, implying a total extinction somewhat higher than the other two estimates.

Orlandini et al. (2000) used emission line ratios to estimate $E(B - V) = 1.54$ mag (from He lines) or $E(B - V) = 1.02$ mag (from H lines). This is based on theoretical predictions of the ratios of the strongest lines in CI Cam. In Be stars and other early OB type stars with dense winds, and likely also in sgB[e]

stars, these lines are subject to effects of non-local thermodynamic equilibrium (NLTE) so this method will not be very reliable.

Robinson et al. (2002) use the 2175 Å interstellar absorption feature in post-outburst *HST* data to measure $E(B - V) = 0.85 \pm 0.05$ mag and $A_V = 2.3 \pm 0.3$ mag; the large error on A_V reflects the uncertainty in the choice of extinction curve parameterised by $R_V = A_V/E(B - V)$.

We can attempt to estimate the Na D equivalent width, although as noted by Munari & Zwitter (1997) this is insensitive for reddened objects as it tends to saturate. It is also complicated by the presence of Na D emission. Fortunately, our echelle spectra obtained in outburst resolve the Na D components as sharp absorptions within the emission line (Fig. 2a). Reconstructing the unabsorbed line profile is obviously uncertain, but assuming it is symmetric we can estimate that the equivalent widths of the two Na D2 (5890 Å[1]) components observed are 0.36 and 0.52 Å. The latter component does appear saturated, so this only provides a lower-limit

---

[1] We note that Munari & Zwitter (1997) incorrectly label the 5890 Å line as Na D1, and 5896 Å as Na D2. Their work is, however, internally consistent; Munari, priv. comm.
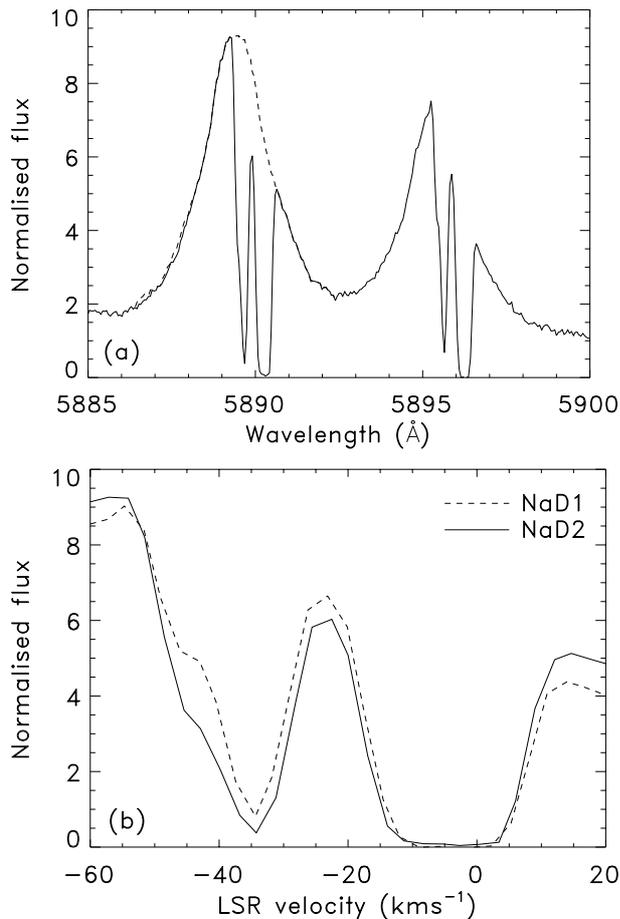
Fig. 2. a) Na D line profiles observed during outburst (1998 April 9). The two interstellar absorption components are clearly visible; the longer wavelength one is saturated. The dashed line shows the reconstructed Na D2 line profile assuming it is symmetrical. **b)** Closeup of the absorption components indicating the velocities with respect to the LSR. The structure in the two lines is consistent. In this direction the LSR velocity is expected to become more negative with distance, so the distance increases to the left. A quantitative distance scale depends on the assumed rotation curve of the Galaxy.

to the reddening. If the profile is actually asymmetric with the same extended blue wing seen in many other lines then this will increase the inferred equivalent width, implying a reddening further above our lower limit. Using the calibration of Munari & Zwitter (1997) for each of the two components we derive a lower limit for the combined reddening of $E(B - V) \gtrsim 0.5$ mag.

Our spectra also reveal several diffuse interstellar bands (DIBs). Our principal reddening calibrator is the $\lambda 5780$ band, using the calibration of Herbig (1993). Using the WHT/UES spectra we measure an EW of 320 ± 30 mÅ implying $E(B - V) = 0.64 \pm 0.06$ mag. The DIB at 5797 Å is too blended with emission lines to reliably measure but we can approximately estimate 140 ± 30 mÅ implying $E(B - V) = 0.9 \pm 0.2$ mag (Herbig 1993). For 5705 Å we measure 110 ± 20 mÅ implying $E(B - V) = 0.49 \pm 0.09$ mag (Herbig 1975). We also use an average of several WHT/ISIS and Skinakas spectra to estimate an equivalent width of 180 ± 30 mÅ for $\lambda 6203$ implying $E(B - V) = 0.62 \pm 0.11$ mag (Herbig 1975), and a central

depth of 0.90–0.97 for the very broad $\lambda 4428$ feature implying $0.3 < E(B - V) < 1.1$ (Krelowski et al. 1987). The 6284 Å line may also be present but is complicated by Telluric absorption. All of the reliable DIB measurements are consistent with $E(B - V) \sim 0.65$ mag as suggested by our principal calibrator, 5780 Å.

To summarise, methods based on interstellar absorption features (2175 Å, Na D, DIBs) all suggest $E(B - V) \sim 0.5$–1.0 mag, and hence visual extinction $A_V \sim 1.5$–3 mag. Methods based on fitting the SED or line ratios, however, favour larger total extinction $A_V \sim 4$ mag. This could arise if the absorption features are only produced in the interstellar medium, and not by local dust extinction, as a consequence of different chemical compositions and/or grain sizes. The SED methods are all model dependent, however, and it may be that the models used are either incorrect or incomplete. This leaves us with some ambiguity about how to deredden spectra of CI Cam. The higher values inferred from SED modelling are most relevant, in the sense that they directly measure the distortion of the broad band spectrum, but they are also model dependent. Measurements based on absorption features are more objective, but do not measure the same thing.

Distance estimates for CI Cam are plagued by even more uncertainty than extinction estimates. A number of works have derived distances of 1–2 kpc (Chkhikvadze 1970; Zorec 1998; Belloni et al. 1999; Clark et al. 2000). All of these, however, involve uncertain assumptions about the luminosity class of the star, or the relation between interstellar absorption and distance. Robinson et al. (2002) challenged this conclusion, arguing for a larger distance. Based on spectroscopic similarities to the largest and most luminous sgB[e] stars they concluded that the distance had to be larger than 2 kpc. Since the line of sight passes well above the warped Galactic plane for 2–6 kpc, they argued that a young object like CI Cam must lie beyond rather than within this distance range. In support of this they note that its radial velocity is consistent with a distance of ~7 kpc, assuming differential Galactic rotation. These arguments, however, make the assumptions that CI Cam is comparable to the most luminous sgB[e] stars, and that it does not have significant peculiar velocity.

More objective constraints on the distance are harder to obtain. We can, however, make one estimate which is almost completely independent of what CI Cam is. As already described, the Na D lines show sharp absorption components. The velocities of these in the local standard of rest (LSR) are -4.5 ± 0.6 km s^{-1} and -34.8 ± 0.4 km s^{-1} for the stronger and weaker components respectively (see Fig. 2b). The stronger component is saturated so it could itself involve multiple components with LSR velocities up to -10 km s^{-1}. The weaker component may also have an additional component in its blue wing at around -45 km s^{-1}; both the Na D1 and Na D2 lines suggest such a feature at this velocity. All of these components are somewhat redshifted with respect to CI Cam, which has an LSR velocity of -51 km s^{-1} (Robinson et al. 2002). It is therefore unlikely they are associated with circumstellar material; much more likely is that they are interstellar gas. If so then we expect them to be moving in the plane in near circular orbits following Galactic rotation, and their velocities can be used to

estimate their distances, and hence a lower limit on the distance of CI Cam. There are obviously uncertainties introduced by non-circular motions and an imperfectly known rotation curve. We estimate distances using the range of rotation curves illustrated by Olling & Merrifield (1998), with the spread in values giving an estimate of the uncertainty in the measurement. The saturated component is clearly associated with the Local Arm, with a maximum velocity $-10\,\mathrm{km\,s^{-1}}$ corresponding to a maximum distance $\sim$1 kpc. We might expect the next feature to correspond to the Perseus Arm at a distance $\sim$2.5 kpc, but the Perseus Arm is not well defined in the direction of CI Cam as our line of sight passes well above the Galactic plane at that point (cf. discussion by Robinson et al. 2002), so it is unsurprising that it produces no absorption feature. The next feature out, at $-35\,\mathrm{km\,s^{-1}}$, is at an implied distance of 3.9–5.6 kpc, and probably corresponds to the next spiral arm out, where our line of sight passes back into the warped outer disc; Cam OB3 (Humphreys et al. 1978) likely belongs to this arm. If the third weak feature, at $-45\,\mathrm{km\,s^{-1}}$, is real and also indicative of Galactic rotation, then it suggests an even greater minimum distance of 6–8 kpc, dependent on the assumed rotation curve.

An alternative empirical approach is to use the radial velocity maps of Brand & Blitz (1993), derived from H II regions and reflection nebulae. This will take account of non-circular motions. If anything, these suggest an even larger distance. The coverage in the direction of CI Cam is sparse, but representative distant objects from their sample (S208, S211 and S212) have LSR velocities between -30 and $-38\,\mathrm{km\,s^{-1}}$ and distance estimates of 5.9–7.6 kpc.

The distance implied for CI Cam by the interstellar features is thus large; it is at least 4 kpc, and may well be beyond 6 kpc. This conclusion is essentially consistent with that derived independently by Robinson et al. (2002) using different methods.

If the closest distance is adopted it is possible that CI Cam could be associated with Cam OB3, possibly as a runaway object. It lies $\sim2\overset{\circ}{.}7$ from the centre of the association; the members identified by Humphreys (1978) lie at up to $1\overset{\circ}{.}2$ from the centre. The distance modulus adopted by Humphreys (1978) was 12.6 (3.3 kpc). CI Cam therefore lies somewhat outside the association, and appears to be further away, but we cannot rule out the possibility that it is a runaway from Cam OB3. Alternatively it could lie beyond the spiral arm containing Cam OB3.

Where it is necessary to assume a value for the reddening in what follows, we either take $E(B-V) = 1.3$ mag ($A_V = 4$ mag) or a range of $0.65 < E(B-V) < 1.4$ ($2.0 < A_V < 4.4$). For the distance, we follow Robinson et al. (2002) in adopting 5 kpc as a representative estimate, although we agree that it could be somewhat larger than this. Where a lower limit is more appropriate we assume $d > 4$ kpc.

5. The nature of the components of CI Cam

CI Cam clearly shows the observational characteristics of the B[e] phenomenon (Allen & Swings 1976; Lamers et al. 1998): strong Balmer emission lines (e.g. Fig. 1), low excitation permitted lines (e.g. Fig. 1), optical forbidden lines of [Fe II] and [O I] (e.g. Fig. 12a) and a strong infrared excess

(Clark et al. 2000); indeed CI Cam has long been considered a B[e] star and was included in the sample of Allen & Swings (1976). In view of the distance estimates discussed above CI Cam clearly falls within the sgB[e] sub-class. The primary characteristic of an sgB[e] star, a luminosity of above $10^4\,L_\odot$ (Lamers et al. 1998) is satisfied for any distance above 0.8 kpc and for the lower limit of 4 kpc that we have argued for above, this rises to $10^{5.4}\,L_\odot$. Robinson et al. (2002) also note spectroscopic similarities to the most luminous sgB[e] stars, consistent with this. The other known types of stars showing the B[e] phenomenon are the pre-main sequence Herbig Ae/Be (HAeB[e]) stars, compact planetary nebula B[e] (cPNB[e]) stars and symbiotic B[e] (symB[e]) stars. HAeB[e] stars typically have luminosities of $\lesssim10^{4.5}\,L_\odot$, are associated with star forming regions and sometimes show evidence of infall, e.g. inverse P Cygni profiles. CI Cam is more luminous than this and exhibits a steep decrease in the IR flux longward of $\sim10\,\mu$m (Clark et al. 2000), indicative of the absence of the cold dust that would be expected around an HAeB[e] star. Lamers et al. (1998) did suggest that CI Cam could be a cPNB[e] star, but as these objects have lower luminosities ($\lesssim10^4\,L_\odot$) this is also ruled out by the distance estimates discussed in Sect. 4. SymB[e] stars are binaries also containing a cool giant which is usually seen in the red or infrared spectrum. Some authors have identified CI Cam as a symbiotic (e.g. Barsukova et al. 2002), but late type features are not seen in CI Cam (except for the report of Miroshnichenko 1995 which was not corroborated by any other observations.) We believe that both the observed spectrum and the high luminosity therefore identify CI Cam as an sgB[e] star, as argued by Robinson et al. (2002).

The sgB[e] class itself includes a range of objects with likely spectral types spanning B0–B9, and luminosities from $10^{4.2}$–$10^{6.1}\,L_\odot$ (Lamers et al. 1998). It is therefore of interest to attempt a more precise classification for CI Cam. We might hope that the detection of photospheric lines from the sgB[e] star would be of great help. In the highest resolution post-outburst spectra of CI Cam, broad absorption wings are seen around higher order Balmer lines, most prominently Hδ and Hϵ (Fig. 3). These may well be photospheric absorption lines from the sgB[e] star. Unfortunately we cannot obtain any detailed diagnostics from these lines because of the heavy contamination we see in the wings of the lines (both in terms of other lines and also probably residual wind emission); hence it is impossible to quantify the underlying photospheric spectrum. Indeed, the photospheric spectrum may be poorly defined for a star with a very high mass loss rate for which a bona fide photospheric radius is hard to determine.

While the spectral type of the star is difficult to determine from the optical spectrum due to heavy contamination by the circumstellar material, the detection of P Cygni profiles in the UV resonance lines with absorption to $\sim1000\,\mathrm{km\,s^{-1}}$ (Robinson et al. 2002) is more useful. By analogy with other sgB[e] stars we expect that the UV P Cygni profiles arise from a hot, polar wind which is similar to that of normal hot supergiants. The outflow velocity implied for CI Cam is directly comparable to that seen for other early B supergiants. The Si IV 1394, 1402 Å doublet functions as a powerful probe of temperature and luminosity for B stars (Walborn et al. 1995).

Fig. 3. Absorption wings surrounding Hδ and Hϵ lines, from 2000 December 1 WHT data. Unmarked lines are mostly Fe II.

Fig. 4. Flux calibrated spectra obtained from FLWO early in outburst and after it. These have been dereddened using the Fitzpatrick (1999) extinction curve assuming $A_V = 4.0$. In outburst, the lines become much stronger and broader, Balmer jump emission appears, and the continuum becomes redder. Note that these are long exposure spectra to ensure that the continuum is well defined, so the stronger emission lines are saturated.

Early-B supergiants show a strong P Cygni wind profile, which evolves into pure absorption for mid-B stars and is absent in late B stars of all luminosity classes – the P Cygni profiles therefore suggest an early B classification. A similar conclusion can be drawn from the presence of P Cygni profiles for the C IV 1549, 51 Å doublet which is seen for supergiants of type B4 or hotter (and is seen in absorption for hot B0–2 dwarfs and giants and cooler supergiants).

By comparison of the optical emission lines with other sgB[e] stars and luminous blue variables (cf. Miroshnichenko 1996), we can further narrow the spectral type to B0–B2, as earlier spectral types show stronger He II emission than the very weak pre-outburst feature that we see, and later types show He I in absorption rather than emission.

To summarise, the "normal" star is an sgB[e] star, with likely spectral type B0–B2 and a luminosity of at least $10^{5.4}$ $L_\odot$, placing it among the hotter, more luminous sgB[e] stars (cf. Robinson et al. 2002).

The nature of the compact object implicated in the outburst is even more uncertain than that of the normal star. It is widely assumed from the X-ray and γ-ray outburst observed that this must be a black hole or neutron star (e.g. Belloni et al. 1999; Robinson et al. 2002). Orlandini et al. (2000), however, have argued for a thermonuclear runaway on the surface of a white dwarf. If the 4 kpc lower limit on the luminosity is correct, however, then the X-ray outburst was extremely luminous, $L_X \gtrsim 2 \times 10^{38}$ erg s^{-1}. This corresponds to the Eddington limit for a neutron star, and for larger distances then a black hole becomes more likely. However, neither the X-ray spectral shape (Orr et al. 1998; Ueda et al. 1998; Revnivtsev et al. 1999; Belloni et al. 1999) nor the lack of rapid X-ray variability (Frontera et al. 1998; Belloni et al. 1999) are typical of accreting black holes or neutron stars. Equally, while there may be a hint of a flaring soft component (Frontera et al. 1998; Ueda et al. 1998), the X-ray spectrum is on the whole quite hard, and not dominated by a supersoft component as might be expected for a high luminosity accreting white dwarf. Consequently the identification must remain uncertain.

6. The spectral flux distribution

Clark et al. (2000) considered the broad band spectral energy distribution from photometric measurements and examined colour changes during the outburst. They found that the source became systematically redder when it was brighter. Given the large contribution of emission lines to the spectrum, however, it is useful to attempt to isolate continuum changes, and quantify the line contribution.

In Fig. 4 we show the first outburst spectrum obtained, which fortunately was flux calibrated, together with a comparable post-outburst one. It is clear that the redder spectrum seen in outburst was not just due to line changes, but that the underlying continuum is redder. We will further discuss the origin of this enhanced continuum emission in Sect. 9.3. There is also an enhancement at higher frequencies as the Balmer jump appears in emission, which explains why the $(U - B)$ index remained constant during outburst (Clark et al. 2000).

In principle, we could also use flux calibrated spectra to estimate how much of the flux in a given bandpass comes from lines. However, in many cases lines are saturated in these spectra, so we instead use unsaturated, but uncalibrated spectra. To do this we construct a flux distribution by interpolating between the outburst JKT points (Hynes et al. 1998) and the mean post-outburst photometry (Clark et al. 2000). We can then multiply such a flux distribution by a continuum normalised spectrum and perform synthetic photometry, iterating until we have a flux distribution such that the synthetic photometry matches the observed values. This is very crude, but for estimating the contribution of lines within a bandpass, the effect of the assumed flux distribution is only to introduce a wavelength dependent weighting within the bandpass, so the results are weakly sensitive to the flux distribution assumed. The contribution from the lines can be estimated by comparing synthetic photometry performed on the flux distribution alone with that performed on the flux distribution multiplied by the normalised spectrum.

The differences in magnitudes which we infer in outburst (1998 April 4) are $\Delta B \sim 0.6$, $\Delta V \sim 0.6$ and $\Delta R \sim 0.9$, and post-outburst $\Delta B \sim 0.08$, $\Delta V \sim 0.10$ and $\Delta R \sim 0.35$. While the quiescent values are fairly small, and hence the quiescent photometry is dominated by continuum, the outburst values can be large; the R band flux, for example, is about 50 percent line emission, due to the strong Hα line. These values are similar to those quoted by Barsukova et al. (2002).

7. Spectral line behaviour

The spectrum of CI Cam has long been known to be rich in emission lines. In outburst, this is even more dramatic, with most lines showing larger equivalent widths, and Balmer and He I lines completely dominating their regions of the spectrum (see Fig. 1). A similarly rich outburst spectrum was seen in the infrared (Clark et al. 1999). We now consider the evolution of selected line strengths and profiles before, during, and after the outburst. We use all the data described earlier together with some measurements reported by Wagner et al. (1998) and Orlandini et al. (2000). Equivalent width lightcurves for a representative range of lines are collated in Fig. 5; these are discussed in turn in the following subsections. No statistical errors have been indicated as the dominant uncertainty is systematic due to contamination from other lines and the uncertain continuum level in such a rich spectrum. Consequently the best indicator of the reliability of a lightcurve is the scatter of the plotted points.

7.1. Hydrogen and helium lines

During outburst H I, He I, and He II lines all brighten dramatically. The increase is much more dramatic than in the continuum, so equivalent widths rise. The rising phase is not observed, except possibly in He II 4686 Å where the earliest observations suggest that the equivalent width peaked around 5 days after the X-ray outburst. Comparison with photometry obtained at this time indicates that this arises because during this period the He II flux was approximately constant while the continuum decayed. For the H I and He I lines, the fact that these lines are already decaying within two days of the X-ray outburst indicates that they originate in a region that can respond to the outburst in less than two days.

There are clearly major differences between the H I and He I behaviours. All the Balmer lines appear to return to approximately their pre-outburst levels within ∼30 days, but the He I lines appear to drop to a factor of 2–10 below this. This effect has been noted previously by Barsukova et al. (1998), Orlandini et al. (2000) and Jaschek & Andrillat (2000) and is clearly real as can be seen in Fig. 1 where spectra before and after the outburst are compared. Further, there appear to be systematic differences between He I lines which are only manifested after the outburst: during outburst the He I EW ratios are similar to those before the outburst, but afterwards they can differ, with He I 7065 Å closest to the pre-outburst level and He I 4713 Å furthest below it. These differences are large, corresponding to a change by a factor of three in the 4713 : 6678 ratio for example, so are not simply due to changes

in the continuum shape. This change in line ratios suggests changes in the physical conditions in the emitting gas; temperatures and/or densities; rather than abundance changes (e.g. due to ejection of material as suggested by Orlandini et al. 2000). An increase in the 6678 : 4471 ratio would be expected from a decrease in temperature, for example (e.g. Osterbrock 1989). Changes in the optical depth could also change ratios, and an increase in the 7065 : 4471 ratio could result from an increase in the optical depth (e.g. Osterbrock 1989). It is unfortunately impossible to be more quantitative for such optically thick NLTE lines. Whatever changes are involved, they should leave the Balmer lines essentially unaffected.

We show a selection of H I, He I, and He II line profiles from outburst WHT/UES data in Fig. 6. Robinson et al. (2002) have already discussed the profiles seen in outburst. The WHT/UES data were obtained a few days earlier than those of Robinson et al. (2002) but are quite similar. They argue that the line profiles, or at least the wings, are kinematic in origin and hence that emission seen to ∼2500 km s^{-1} indicates the velocity of the hydrogen and helium emitting material outflowing from the sgB[e] star. There are alternative possibilities to be considered, however. The broad wings to the lines are most prominent during outburst so may be associated with material ejected from the accreted compact object rather than from the sgB[e] star. Given that these lines are likely formed in regions of high optical depth (see Sect. 7.4), incoherent Thomson scattering may also broaden the lines significantly; this has been proposed for other sgB[e] stars (Zickgraf et al. 1986). Scattering would be expected to be symmetric, but the observed profiles can be interpreted as the sum of a broad blue shifted component and a narrower component at rest (Robinson et al. 2002). These authors obtained a satisfactory fit to the profiles with a double Gaussian, with the a narrow rest component (*FWHM* 50–85 km s^{-1}) and a broad component (*FWHM* ∼160 km s^{-1}) blue-shifted by ∼60 km s^{-1}. We find similar results from our WHT/UES spectra, although we do not obtain a satisfactory fit with a double Gaussian model to the He I lines. This is likely due to the inadequacy of a Gaussian fit rather than an intrinsic asymmetry. A double Voigt profile fit, for example, gives extra freedom while still using symmetric components and works much better. There is some sensitivity of the fit parameters to whether a Gaussian or Voigt profile is used, even when both fit well. For all fits to all lines we obtain blue shifts of 40–110 km s^{-1}, and *FWHM* of 60–90 km s^{-1} and 140–230 km s^{-1} for the narrow and broad components respectively, consistent with the estimates of Robinson et al. (2002). Only the blue shift, 40–110 km s^{-1}, needs to be kinematic and we then have much lower velocities in the hydrogen and helium emission regions, more comparable to the velocities inferred for metallic lines. It remains possible that the width of the broad components is kinematic however.

During the outburst, large changes are seen in these line profiles. This is illustrated for Hα and He I 6678 Å in Fig. 7. At the earliest epoch (1998 April 3) both lines are extremely broad and show structure not discernible at later times. Emission is clearly seen up to 2500 km s^{-1} in both lines, and possibly extends to ∼5000 km s^{-1} in the blue wing of Hα, although this is contaminated by other lines. The Hα profile in fact looks
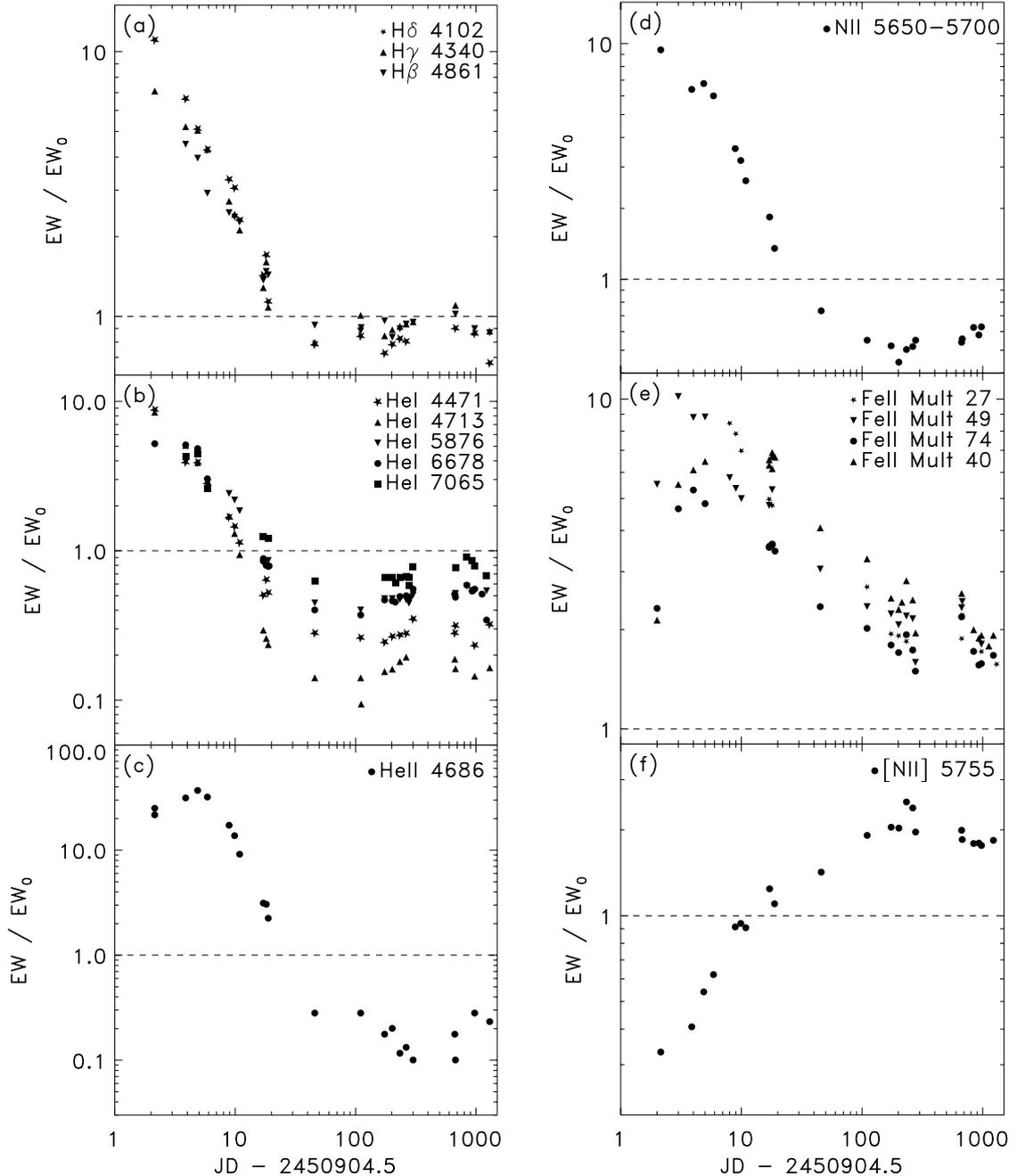
Fig. 5. Equivalent width evolution of various lines during and after the outburst. All equivalent widths have been normalised to pre-outburst levels, shown as a dashed line, except where noted. All points correspond to individual nights except for the 1998 Sept–Dec FLWO data for which monthly averages have been plotted as the evolution is slow by this time. The zero-point of time corresponds to the peak of the X-ray outburst. **a)** Balmer line evolution. Hα is not plotted because it is so strong as to be unreliable in many spectra. **b)** He I evolution. Lines at 4921 Å and 5015 Å are omitted as they are blended with strong Fe II lines in most spectra. **c)** The He II 4686 Å evolution. **d)** Evolution of 5650–5700 Å blend. This is likely dominated by N II 5676,5686 at the peak. **e)** Evolution of Fe II lines. The spectral lines used were: $\lambda\lambda4233$, 4303, 4351, 4385, 4416 (multiplet 27); $\lambda\lambda6432$, 6516 (multiplet 40); $\lambda\lambda5197$, 5234, 5275, 5316, 5325, 5425 (multiplet 49); and $\lambda\lambda6238$, 6248, 6416, 6456 (multiplet 74). For each multiplet the sum of equivalent widths has been taken. For multiplets 40, 49 and 74 this was normalised to the equivalent sum before the outburst. These multiplets are then in approximate agreement by the end of the period observed (around day 1000), so multiplet 27, for which no reliable pre-outburst measurements are possible, was also arbitrarily normalised to agree with them. The rise between the first few observations is definitely real, being seen in all 12 lines for which measurements could be made. **f)** Evolution of [N II] 5755 Å.

remarkably like that of Hen S134, a near pole-on sgB[e] star in the LMC (Zickgraf et al. 1986). Both show a low-velocity blueshifted "notch", although the overall width of the Hα line is much larger for CI Cam. For Hen S134, Zickgraf et al. (1986) suggested that the notch was due to an unresolved absorption feature. That might also be true for CI Cam, but the He I
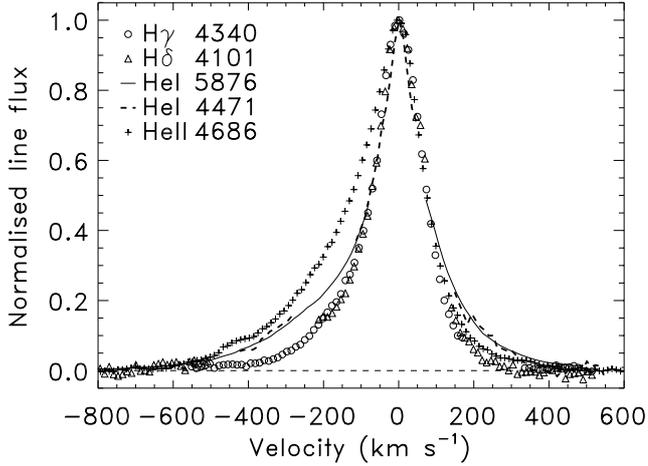
Fig. 6. Profiles of the stronger hydrogen and helium lines in outburst based on WHT/UES data from 1998 April 9. The profiles have been rebinned by a factor of four for clarity. Regions contaminated by other lines have been omitted.

profile suggests an alternative explanation. The latter shows inflections in both the blue and red wings. In fact this line clearly suggests two distinct components: a narrow line at rest and a broad blue-shifted line; the Hα profile may arise the same way, but with a broader rest component. This is of course exactly the decomposition that was applied successfully to later spectra and suggests that rather than using such a two-component fit as a convenient parameterisation of an asymmetric profile, we can actually take it more literally: there really are two distinct emission regions. Furthermore, fitting the same two component model to the 1998 April 3 He I profile gives very similar results to the later spectra with a component separation of ~50 km s^{-1} and a narrow component *FWHM* of ~75 km s^{-1}. The main difference is that the broad component in the earlier spectrum is much broader with a *FWHM* ~750 km s^{-1}. In fact, there is a hint that the narrow component of Hα on April 3 may itself be more complex. The distortion of the peak may indicate that it contains two unresolved components. This structure is repeatable over all of the individual spectra, obtained on this night, and the line peak was not saturated.

In quiescence, the weaker hydrogen and helium lines become narrower, approaching the width of the iron lines (see Figs. 7–9). These lines can never be expected to be as narrow as the iron lines as the thermal widths will be larger for lighter elements. Robinson et al. (2002) observed broadening of 3.1 km s^{-1} for the Fe II lines, and also estimated a temperature of the iron emission region of 8000 K, corresponding to a thermal component of broadening of 1.9 km s^{-1}. The latter will correspond to ~14 km s^{-1} for hydrogen lines. Figure 9 shows the observed Hδ profile (which should be less affected by optical depth effects than stronger lines) from 2000 December 1, well after the H I lines had stabilised after the outburst. We have constructed a simple model profile by taking a square topped profile extending to ±32 km s^{-1} (the model Robinson et al. 2002 used for the metallic profiles) and broadened it by ~14 km s^{-1}. This model profile is somewhat narrower than the observed Hδ profile, but the difference is not dramatic, so
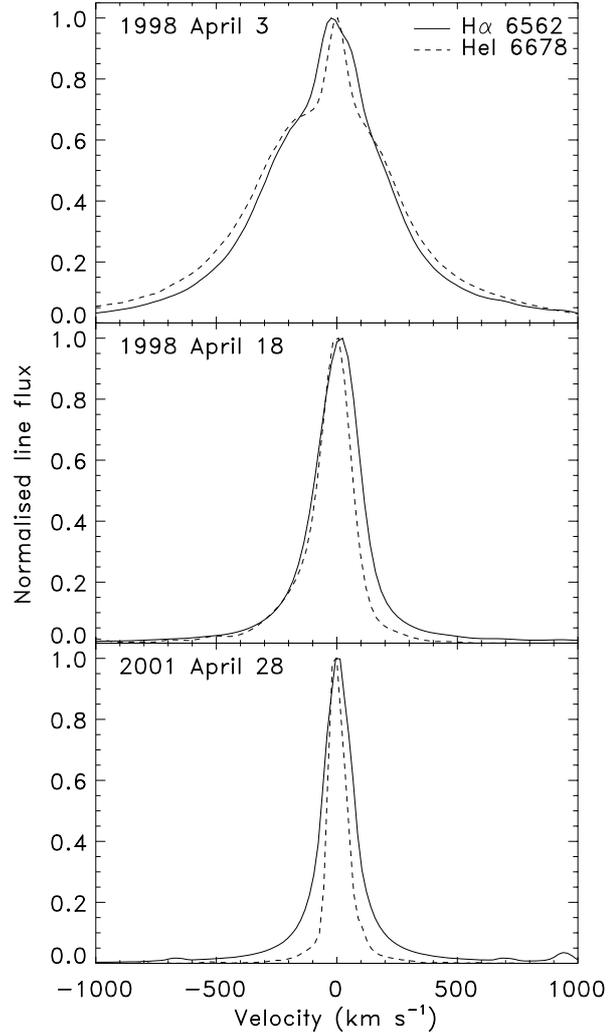
Fig. 7. Changes in the profiles of Hα and He I 6678 Å from outburst to quiescence. There is clearly a dramatic change in the width of the lines, and the early profiles also show a two component structure.

it is plausible that the underlying H I kinematics are similar to the Fe II lines. Some extra broadening may arise from a higher temperature in the hydrogen emission region and/or radiative transfer effects.

It appears that He II 4686 Å is still detectable after the outburst, as noted by Barsukova et al. (2002). A close examination of the pre-outburst OHP spectra reveals that it was also present then at a *higher* level, albeit still weak, indicating that it is not simply a remnant of the outburst. This is somewhat surprising and another contaminating line cannot be ruled out. Such a line would, however, have to share the property of the He I and N II lines of being weaker after the outburst than before, which is not consistent with Fe II line behaviour, for example. At least one other sgB[e] star shows He II emission (the luminous B0 star Hen S134; Zickgraf et al. 1986), however, so this is not unprecedented, and is further evidence that CI Cam is among the hottest sgB[e] stars.
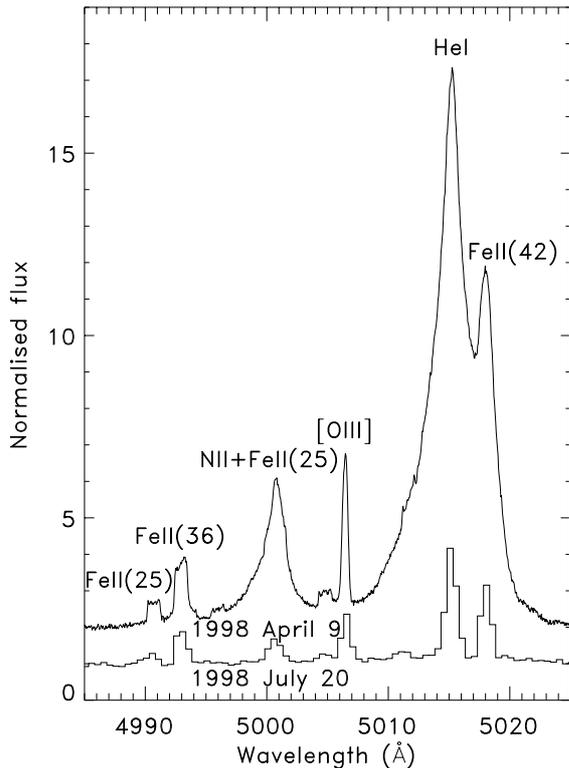
Fig. 8. Change in the width of the He I 5015 Å line between outburst and post-outburst phases. Note the similar behaviour of the N II 5001 Å line. The upper spectrum has been offset by one unit vertically.
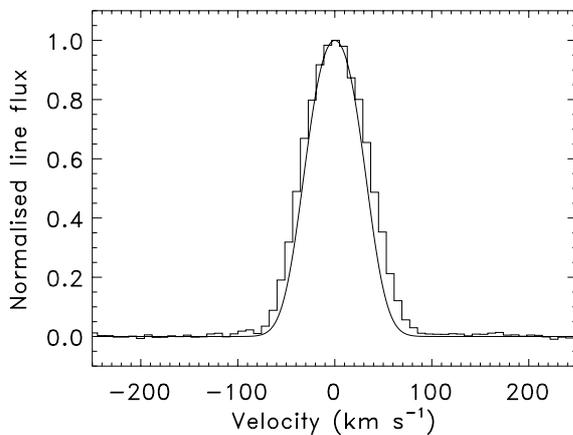
Fig. 9. Hδ profile from 2000 December 1. The underlying absorption (see Sect. 5) is much broader than this, so provides an effectively flat background which has been subtracted. The histogram is the data, the smooth line is a square profile extending to ± 32 km s^{-1} broadened by 14 km s^{-1}. The model profile has also had instrumental broadening applied, although this is a smaller effect.

7.2. The Bowen blend

A common feature of the spectra of X-ray binaries is the Bowen blend, a mixture predominantly of N III and C III lines spanning ~4635–4650 (McClintock et al. 1975). This feature does also appear to be seen in CI Cam, but can only be discerned in the WHT/UES outburst spectra. These data are shown in Fig. 10. Features are seen corresponding to first two of the
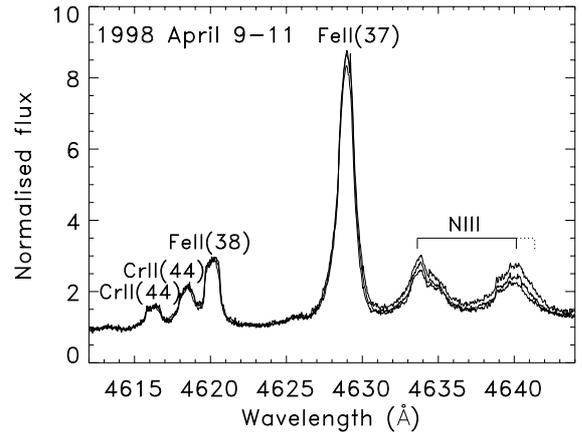
Fig. 10. N III Bowen fluorescence lines seen in outburst. Three normalised spectra are plotted corresponding to the three nights observed. The only major changes are in the Bowen features which become systematically fainter with time. The three N III components are indicated, although the 4642 Å line, indicated by the dashed line, is not clearly visible and may be weaker and/or unresolved.

N III 4634, 4641, 4642 Å lines; the third may be present but unresolved from 4641 Å. These features appear broader than Fe II and Cr II lines in the same region and are clearly declining much faster. It therefore seems likely that these are the N III Bowen fluorescence lines. The adjacent echelle order also appears to show the C III 4647, 4650, 4651 Å lines which show similar properties. Neither set of lines appear to be present after the outburst, although the post-outburst data are of lower resolution and quality.

7.3. The 5650–5700 Å blend

There are several lines between 5650 and 5700 Å which are dramatically enhanced during the outburst. In many spectra these are blended with other lines in the region which are less variable. The blend appears to be composed of N II, Sc II, and Fe II lines (Fig. 11); the variable ones are likely allowed N II lines from multiplet 73 at 5676, 5686 Å. The strongest predicted line from this multiplet, 5679 Å, is not clearly seen, but may be present at a lower level and poorly resolved from the wing of the 5676 Å line. The evolution of the total equivalent width of the blend is plotted in Fig. 5d and shows a rather similar behaviour to the He I lines, with a lower flux after outburst than before.

7.4. Near-IR oxygen lines

There are a number of important emission lines of O I detected in the near-IR spectrum. These were not observed often enough to construct lightcurves, but they still reveal useful information. The strongest is O I 8446 Å. This has an equivalent width of 41 Å before the outburst and 57 Å after it. It is very strong but as discussed by Grandi (1980) there are several possible reasons for this. Our observations yield rather similar results to those of Chakrabarty & Roche (1997) for GX 1+4, so we come to similar conclusions: that O I emission is produced by
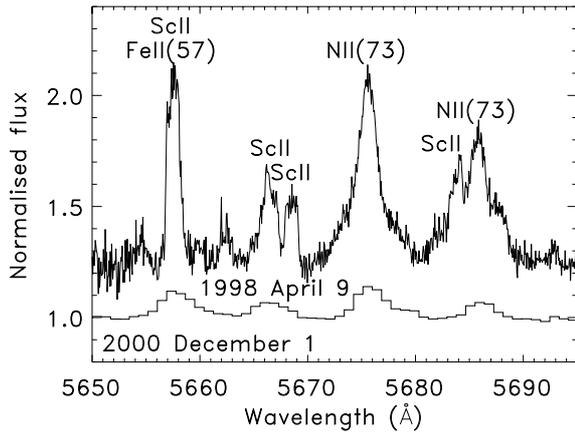
Fig. 11. The 5650–5700 Å blend. This appears to be a mix of N II, Sc II and Fe II lines. In the earliest outburst spectra the blend is unresolved, but it is clear that the N II 5676 Å line dominates, more so than in the spectra plotted here. The N II 5679 Å line should also be present; it may be detected in the red wing of the 5676 Å line. The upper spectrum has been offset by 0.25 units vertically.

H I Lyβ fluorescence; Clark et al. (1999) came to the same conclusion independently from the 1.13 and 1.32 μm infrared lines. We find that the O I 7774 Å line is much weaker than 8446 Å ($EW \sim 2.6$ Å before the outburst and 4.2 Å afterwards), corresponding to dereddened flux ratios (7774:8446) after the outburst of order 0.07–0.10 accounting for uncertainty in reddening. This rules out production of 8446 Å by recombination or collisional excitation, instead favouring a fluorescence process. Continuum fluorescence would also predict O I 7254 Å and 7990 Å, neither of which are detectable before or after the outburst, arguing against this interpretation. The most likely explanation is then fluorescence by H I Lyβ. This process requires a gas which is optically thick to Hα, and the ratio of 8446 Å to Hα can be used to estimate the Hα escape probability (see Grandi 1980). We estimate a dereddened flux ratio (8446:Hα) after the outburst of 0.07–0.12 and hence an Hα escape probability of $(1.5-2.5) \times 10^{-4}$, implying a very high optical depth in Hα.

7.5. Metallic lines

CI Cam was dubbed "the iron star" by Downes (1984) and this is an appropriate designation. The spectrum before, during, and after the outburst is rich in Fe II lines, in many cases blended in all but the highest resolution spectra. It is impractical to show the evolution of all lines because of both the large number of lines and also blending problems. In Fig. 5e we compile results from four multiplets covering a range of wavelengths and excitations. Lines from each multiplet that cannot be reliably deblended or that are sampled by few spectra are excluded. It is clear that the decay from outburst is extended; it may still be continuing even in the most recent observations. This is consistent with the observation that the iron lines appear stronger in post-outburst spectra than in pre-outburst ones (if they are still enhanced above their "true" quiescent level). Minor differences appear between multiplets,

e.g. compare multiplets 40 and 49. There is no systematic trend either with wavelength or with excitation, however, and the origin of the difference is unclear. The rise in the early stages of the outburst is real, as it involves a difference of a factor of two and is repeated across 12 lines for which measurements could be made over 1998 April 3–6. It suggests that the iron *EW* peaked around day 3–10 of the outburst.

Iron is by no means the only metallic species in the spectrum. For example, Robinson et al. (2002) also identify permitted lines of Na I, Mg I, Si II, Ca II, Sc II, Ti II, and Cr II as well as C, N, and O lines. The behaviour of these lines can differ dramatically. For example Fig. 12 shows a selection of Fe II and Ti II lines during and after the outburst. The Ti II lines are clearly much more variable than the Fe II lines and are almost undetectable in quiescence. This is puzzling as the Fe II lines shown are of *higher* excitation than the Ti II lines (5.6 eV for Fe II; 4.0 eV for Ti II.), and the ionisation potential of Fe II, 7.9 eV, is also higher than that of Ti II, 6.8 eV. Possibly the Ti II lines are formed in a different region to Fe II. Cr II lines may also virtually disappear in quiescence, although all are quite weak even in outburst.

The profiles of the metallic lines have been characterised by Robinson et al. (2002) as a square topped profile extending to ± 32 km s^{-1} and subject to a small thermal broadening. They attributed this to a uniformly expanding spherical shell (Fig. 13a). We will discuss these lines in the context of sgB[e] models in Sect. 9.1, but here will note a complication and an alternative explanation. The complication is that while a square topped profile clearly provided a good description of the profiles at the time of the Robinson et al. (2002) observations, this is not adequate at other times. Figure 12 shows two segments of our 1998 April 9 WHT/UES outburst spectrum, together with post-outburst counterparts. The latter are at lower resolution, but are still sufficient to show deviations from the flat topped profile; the Fe II 4297 Å line clearly shows double peaks, or a central depression. This is essentially the same as the [Fe II] 4287 Å line, but the latter is also double peaked in outburst. Other lines in this spectrum show similar profiles, so this is not just due to noise. The problem is worse than this, however, as can be seen in Fig. 12b. This shows our WHT/UES spectrum of the region used for Fig. 7 of Robinson et al. (2002). Two lines in particular, Cr II 5421 Å and Fe I 5430 Å, both of which showed flat topped profiles in the data of Robinson et al. (2002) are actually double peaked at our earlier epoch. Thus the deviation from a flat topped profile cannot simply be a post-outburst effect, and the profiles appear to evolve from a double peaked to flat to double peaked form through and after the outburst. Consequently the flat topped profiles seem to be the exception rather than the norm, and the variations seen suggest some deviation from spherical symmetry. We suggest that the underlying symmetry is axial rather than spherical, but that our viewing angle is along the axis (i.e. we see the star pole-on). If we view any equatorial section of a spherical outflow pole-on then the profile will be rectangular, with narrower equatorial outflows producing narrower profiles (Fig. 13b). If emission from the equatorial outflow varies with latitude then variations from a flat top would be seen, and a central depression would imply less emission near the equatorial plane (Fig. 13c).
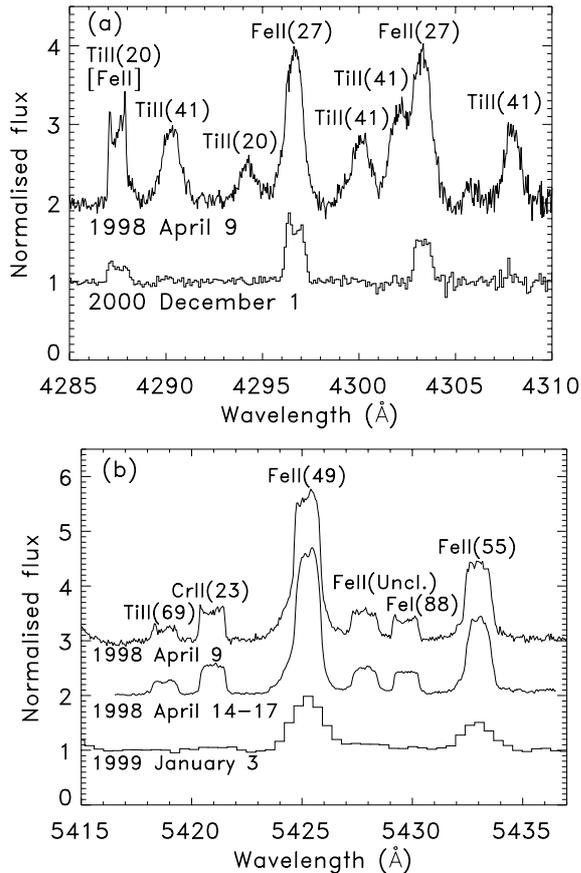
Fig. 12. a) Changes in metallic lines from outburst to quiescence. Ti II lines are much more variable than Fe II lines and are virtually undetectable in quiescence. The Fe II profiles change, being rounded in outburst but concave in quiescence (like [Fe II] lines). Note that the Fe II line at 4297 Å in particular does not become square topped in quiescence. The upper spectrum has been offset by one unit vertically. **b)** Outburst spectrum of 5415–5437 Å region. The spectrum from April 14–17 is reproduced from Fig. 7 of Robinson et al. (2002). Note how the concave tops of the Cr II and Fe I lines in the earliest spectrum later become flat tops

7.6. Forbidden lines

A number of forbidden transitions are observed in [O I], [O III], [N II] and [Fe II]. These are a rather heterogeneous selection of lines spanning a range of ionisation stages and showing very diverse behaviours. As already noted by Robinson et al. (2002), [N II] and [O III] lines are extremely narrow, more so than any permitted lines (e.g. Fig. 8). [O I] and [Fe II] lines, however, exhibit square-edged profiles similar to the Fe II lines, although typically with a more pronounced central depression (e.g. Fig. 12a). In the context of the equatorial outflow geometry suggested for the Fe II lines, a deeper central depression would imply less emission close to the equatorial plane. This makes sense, as the density is expected to be higher there and so forbidden lines may well only be seen from higher altitude, lower density, layers.

The line changes with time differ between species too. Unfortunately, many of the lines are weak and/or blended with other lines, principally of Fe II. The only line well suited to
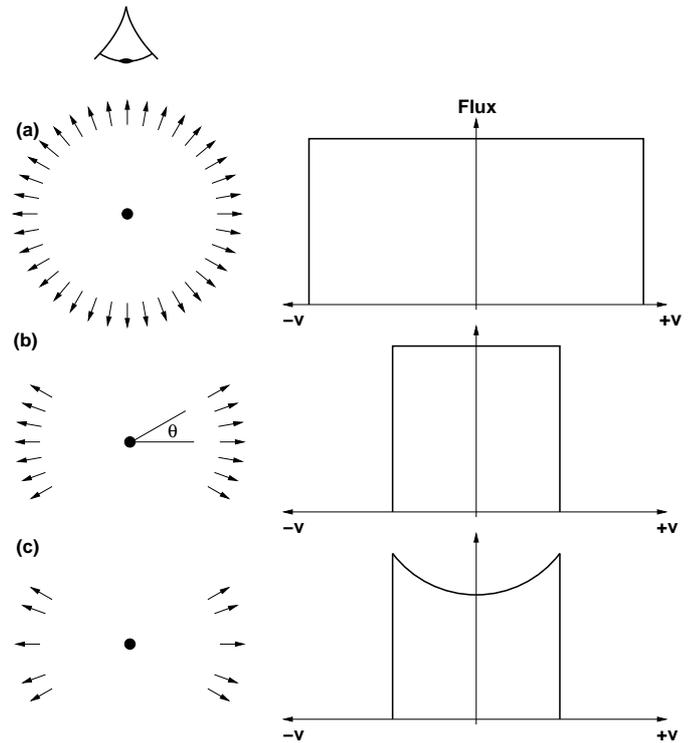
Fig. 13. Illustrative optically thin profiles for different outflow geometries. The viewing angle is taken to be from the top of the page, i.e. pole-on. **a)** A spherically symmetric outflow produces a square profile extending to $\pm V_{\text{term}}$. **b)** An equatorial section of a spherical outflow also produces a square profile (when viewed pole-on), but narrower, extending to $\pm V_{\text{term}} \sin \theta$. **c)** If the outflow is non uniform, with less emission closer to the equatorial plane, then a central depression is created, because there is less low velocity emission.

quantitative analysis is [N II] 5755 Å, as it is strong and unblended. The equivalent width evolution of this line is shown in Fig. 5f. The early evolution ($\lesssim 10$ days) is roughly consistent with a constant line flux, with the equivalent width increasing as the continuum fades. Comparison with outburst photometry (Clark et al. 2000), after correcting for the increased contribution of the lines to broad band flux (Sect. 6), indicates that this outburst line flux is comparable to that seen in 1998 January. Barsukova et al. (2002) note that the line flux does increase modestly around 50–250 days after outburst, then decays again. The decay can clearly be seen in Fig. 5f, although the rise is hard to distinguish from that due to the decreasing continuum flux without flux calibrated spectra.

The [O III] 5007 Å line also exhibits a narrow profile but is clearly stronger in outburst than after it (Fig. 8). The 4959 Å line behaves in a similar way. These lines are difficult to measure in most spectra as they are weak and blended, but it is clear that the outburst flux is much greater than pre-outburst and that after the outburst they decline, but like [N II], they do not appear to have dropped to the pre-outburst level. For example, for [O III] 5007 Å, the pre-outburst *EW* is difficult to measure but ~0.25 Å. On 1998 April 11 it had an *EW* of 2.0 Å and by 1998 July 20 this had dropped to 1.1 Å. As late as 2001 October 23 it was still $\gtrsim 0.8$ Å. The decline in *EW* from 2000 April to July corresponds to a decrease of about a factor

of three in line flux. Since the [O III] lines have very long recombination times, this implies that significant collisional de-excitation must be occurring, possibly when the radio ejecta reach the line formation region. Assuming an expansion velocity of $\sim 5000 \, \text{km s}^{-1}$, then a reduction of a factor of three within ~ 100 days implies that most of the [O III] emission originates within ~ 300 AU.

[Fe II] lines also strengthen moderately during outburst (e.g. Fig. 12a) and [O I] lines increase enormously, being almost undetectable before and after the outburst.

8. Short term spectral variability

There have been some claims of short term variability in CI Cam during outburst. At X-ray energies Frontera et al. (1998) found with *Beppo-SAX* that the 0.5–1.0 keV lightcurve showed significant variations on ~ 100 s timescales on 1998 April 9–10. They found no significant variation from a smooth decay in the simultaneous 1.5–10 keV data however, nor were any variations seen on April 3. Ueda et al. (1998) examined *ASCA* data from 1998 April 3–4. They also found that there was no variability above 1 keV, but that soft flares were seen below 1 keV on timescales of a few hours. Belloni et al. (1999) examined *RXTE* data spanning April 1–9 and found no evidence for any variation other than a smooth decay at any time. The short term X-ray variability thus appears confined to flares in the soft ($\lesssim 1$ keV) band.

Optical variability appears sporadic too. Frontera et al. (1998) also found evidence for 0.3 mag optical flickering on hour timescales on April 6, but not in later observations spanning April 10–26. Clark et al. (2000) examined photometry from April 13 and 19 and found no variations with amplitude greater than 1 percent.

The McDonald spectra obtained during the decline from outburst were taken as a series of short exposures to facilitate studies of line variability. Because a relatively narrow slit was used, however, there are significant slit losses. Fortunately, as noted above (Clark et al. 2000), there was no detectable short-term variability in simultaneous *R* band photometry, so we chose to normalise each spectrum before extracting emission line lightcurves; these lightcurves are effectively equivalent widths. We find no evidence for variability on timescales from 3 min to ~ 2 hr in Hα or Fe II lines. Formally we find rms scatters in the lightcurves of 1.1–1.6 percent in Hα and 0.8–1.5 percent for a composite of several iron lines. The one line that may exhibit short term variability is He I 6678 Å. This shows 1.9, 4.9 and 3.5 percent rms variations on 1998 April 18, 19 and 20 respectively. On the latter two nights there is clearly a systematic variation. To be sure this is not an artifact we have renormalised the continuum using just the 6648–6663 and 6693–6708 Å regions and recentered the line in each spectrum by cross-correlating the line profiles with an average. None of these changes affect the result: this line appears to show real variability. The case is most persuasive on the last night. There is a clear overall rise in the linestrength of ~ 10 percent over <3 hours, shown in Fig. 14. This is in the opposite direction to the overall decline in the linestrength and much larger than expected from the changes in the continuum strength alone
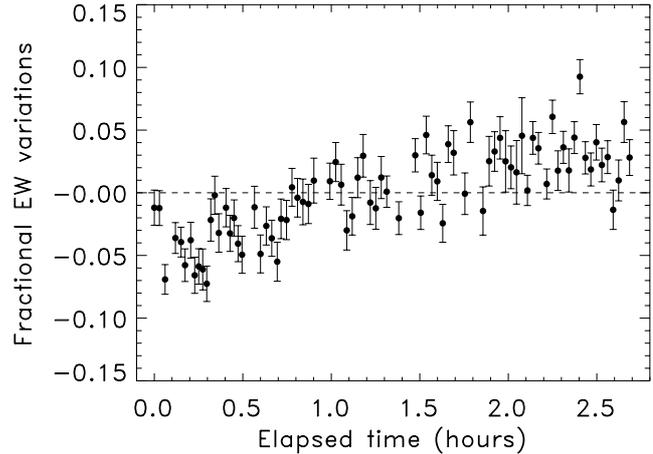
Fig. 14. Change in the strength of the He I 6678 Å line in McDonald spectra from 1998 April 20. Spectra were normalised to a flat continuum which was then subtracted. Integrated line fluxes are plotted as fractional variations about the mean. Error bars are formal errors obtained in extracting one-dimensional spectra and do not include additional uncertainties that may be introduced by normalisation of the spectra.

(e-folding decay time ~ 24 days at this time; Clark et al. 2000). We have also constructed rms spectra for each night and compared them with the average spectra. These suggest the same conclusion as the lightcurves; the only feature that seems to show significant variability is the He I line on the second and third nights.

We also examined the FLWO data from 1998 April 3 in the same way. The rms spectrum shows no variable features other than Telluric bands. The line strengths for Hα and He I 6678 Å show an rms scatter of 1.8 percent and 1.2 percent respectively with no systematic trend. We believe this represents a null detection of variability on this night.

9. Discussion

9.1. CI Cam as an sgB[e] star

It is clear that the X-ray outburst was associated with dramatic changes in the spectrum of CI Cam. Having identified it as an sgB[e] star, however, it will prove useful to first compare it with the small number of other stars of this class and see how much of its "unusual" behaviour, is typical of these objects, and what requires additional input from a compact object.

Robinson et al. (2002) infer a predominantly spherical geometry for the outflow from CI Cam. Several components are suggested. A cool, low velocity (32 km s^{-1}) wind gives rise to the many iron lines and the square profiles of these lines suggested that this component is spherical. Multiple higher velocity components (>1000 km s^{-1}) are suggested by hydrogen and helium lines, and by the UV resonance lines. This picture has several problems as noted by Robinson et al. (2002), principally i) it is unclear how several near-spherical winds can co-exist with very different velocities and ionisations; and ii) the quiescent X-ray luminosity is very low for a compact object continually burrowing through a dense, spherical outflow.

This picture is also rather at odds with existing models of sgB[e] stars (Zickgraf et al. 1985, 1986; Oudmaijer et al. 1998). The structure inferred from other systems is of a two-component wind which is far from spherical. A rarefied, hot, high velocity wind dominates in the polar regions and is responsible for the UV lines often seen with P Cygni profiles. This wind is identical to the winds of normal early-type supergiants. Other lines are attributed to a cooler, denser wind concentrated in the equatorial regions that is not present in normal supergiants. The nature and origin of this equatorial material remain unclear, and it is probably quite different to the discs around classical Be stars. Can CI Cam be fitted into this framework?

The interpretation of the UV lines seen in CI Cam is most straightforward. These show broad P Cygni lines typical of supergiant winds. They can be associated with the hot, high velocity, polar outflow, and we essentially agree with Robinson et al. (2002) on the interpretation of these lines.

The hydrogen and helium lines are more problematic, however. In outburst, these lines are broad and asymmetric, with blue-shifted emission extending to $\gtrsim 2500\,\mathrm{km\,s^{-1}}$, but with no detectable absorption components. Robinson et al. (2002) associate these lines with a high-velocity, weakly collimated outflow from the sgB[e] star. It is unclear where this could be situated, however: if it originated from the same region responsible for the UV lines we might expect P Cygni line profiles, as seen in HD 87643 (Oudmaijer et al. 1998). The latter object may be rather different to other sgB[e] stars with a higher H I column density in the polar wind. In most sgB[e] stars, hydrogen and helium emission is instead attributed to the equatorial component, and hence relatively low velocities should be involved, as is seen in the iron lines. In fact, a clue that the hydrogen, helium and iron lines are all associated with the same region, or regions, is provided by similarities of the line profiles. Robinson et al. (2002) associate Fe II lines with a very different region to the hydrogen and helium lines, but they also note that "*The stronger [iron] lines have more rounded profiles, becoming almost Gaussian in shape as the lines become stronger, and the very strongest lines have an extended blue wing*". Another way to put this is that the strongest lines become more akin to hydrogen and helium lines. While the rounded profiles could indicate radiative transfer effects, the presence of asymmetry in the Fe II lines suggests that the same rest and blue-shifted components are present in the iron lines as are seen in hydrogen and helium profiles. If the strongest, optically thickest iron lines look like hydrogen lines, then the corollary is that the weakest, optically thinnest hydrogen and helium lines should look like iron lines. This does seem to be the case, as demonstrated in Sect. 7.1 and Fig. 9.

The decomposition of the hydrogen and helium lines into two clear components suggests that two distinct regions are involved during outburst. The narrow rest component dominates in the iron lines and is also important in the hydrogen and helium lines. A second broad, blue-shifted component is present in hydrogen and helium lines, and weakly detectable in the strongest iron lines. The narrower, rest component is likely the same component as seen in quiescence, and in other sgB[e] stars, originating from the equatorial outflow.

The profiles seen in H I and He I are very different to the Fe II lines, but the former are broadened by larger thermal widths and incoherent Thomson scattering, as suggested by Zickgraf et al. (1986) for other sgB[e] stars. The strong, broad, blue-shifted component is a feature of the outburst and may not be associated with the outflow from the sgB[e] star at all. We will discuss this possibility further in the following section.

Associating the iron lines with the equatorial material conflicts with the interpretation of their profiles offered by Robinson et al. (2002). They argue that the rectangular profiles allow little deviation from spherical symmetry and no significant rotational velocity. As we have discussed in Sect. 7.5, however, large deviations from spherical geometry are possible in one case: that an equatorial outflow is viewed pole-on. A pole-on equatorial outflow can also explain the apparent lack of rotational velocities, as the *projected* rotational velocity could be very low, and the intrinsic rotational velocity in regions of the disc where Fe II can arise is in any case likely to be very low.

As a further argument for the presence of a spherical low velocity wind, Robinson et al. (2002) claim on the basis of the scaling relation of Bjorkman (1998) that dust can condense in this wind and that an equatorial outflow is therefore not required for the production of dust. The scaling relation of Bjorkman (1998) is based on the argument that the density of wind compressed outflows in sgB[e] stars at radii where the wind is cool enough for dust to condense is ~equal to those of post-AGB stars (which do form dust) and therefore that it is possible for dust to condense in such outflows. However, the scaling relation does not allow for the fact that the winds in post-AGB stars are significantly enhanced in species such as Si and C (via dredge up) which form dust up to a factor of ~10 times more easily relative to the winds from sgB[e] stars. Additionally, the mass loss for the sgB[e] star is calculated from the base density of the outflow at the surface of the star and the *terminal velocity* of the outflow, rather than the velocity of the outflow *at the surface of the star*. This will also serve to overestimate the density of the outflow at the dust condensation radius. Combining the 2 arguments we estimate that the density is likely to be 2–3 orders of magnitude too small to allow dust to condense (J. Porter, priv. comm.). While this does not a priori argue against the presence of a quasi-spherical wind resulting in the Fe II line profiles it *does* demonstrate that dust cannot condense in it and that a region of higher density – whether an equatorial outflow or dense ejecta – is required for condensation. Robinson et al. (2002) additionally argue that the presence of a resolved, circular dust shell (Traub et al. 1998) is consistent with their interpretation, but we note that if a disc is viewed pole-on then dust in the outer regions of the disc will produce the same apparent structure.

Forbidden lines are a rather heterogeneous mixture, but broadly divide into two types. Narrow lines ([N II], [O III]) are formed in a region of very low bulk, turbulent and/or thermal velocities. This probably places them outside the two component outflow from the sgB[e] star, and they may be a remnant of an earlier phase of evolution of one of the stars (cf. Oudmaijer et al. 1998). The [Fe II] lines show profiles similar to the Fe II lines, but with a more pronounced central

depression. As discussed in Sect. 7.6, this suggests that these lines may be formed in the upper layers of the same equatorial material responsible for Fe ɪɪ; [O ɪ] lines are likely formed in the same region.

To summarise, by analogy to other known sgB[e] stars we suggest that when the system is not in outburst, the strongest optical permitted lines (H ɪ, He ɪ, Fe ɪɪ, and others) and some forbidden lines ([Fe ɪɪ], [O ɪ]) arise in an equatorially concentrated region, whether a quasi-Keplerian disc (e.g. Okazaki 2001), a hybrid disc with a slow radial expansion velocity, or even in a radiation driven disc wind such as is suggested in the Galactic sgB[e] star HD 87643 (Oudmaijer et al. 1998). UV P Cygni lines originate from a hotter, higher velocity polar outflow of much lower density. The whole structure is viewed close to pole-on, hence disc lines have rather low velocities as both rotational and expansion velocities would be mainly directed in the equatorial plane. Finally the narrow forbidden lines ([N ɪɪ], [O ɪɪɪ]) come from a much more extended and near stationary region.

Our suggested model does depend on viewing the source near pole-on. There are several independent lines of evidence to support this, suggesting that CI Cam is seen at a lower inclination than many sgB[e] stars.

1. Most sgB[e] stars show low velocity blueshifted absorption in their Balmer line profiles (Zickgraf et al. 1985, 1986; Oudmaijer et al. 1998). This can be interpreted as due to absorption by the slow equatorial wind component. No such absorption is seen in CI Cam suggesting that the inclination is low enough that our line of sight does not pass through the slow wind.
2. sgB[e] stars are expected to show significant polarisation changes through Hα. The observations of HD 87643 are qualitatively similar to what is expected for a rotating, expanding disc (Oudmaijer et al. 1998). In CI Cam no polarisation changes are seen through the lines (Ikeda et al. 2000). In the models of Wood et al. (1993) the polarisation decreases with inclination, so a lack of line polarisation also supports a low inclination. In addition, the outburst observations of Ikeda et al. (2000) showed a continuum polarisation consistent with surrounding field stars, and hence with purely interstellar polarisation. This is also as expected for a nearly pole-on disc.
3. We have argued above that dust cannot form in a spherical shell and that it must be associated with the outer disc. The near perfectly circular resolved infrared image then suggests that this disc must be viewed pole-on.

It therefore seems plausible that CI Cam is a pole-on sgB[e] star. Such a model is consistent with the properties of both the optical and UV spectra.

9.2. The nature of the outburst

We now move on to discuss the role of the compact object. Its nature obviously has some bearing on this discussion. The X-ray outburst was very short, much shorter than typical of soft X-ray transients (SXTs). This, together with the radio emission from an expanding remnant (Mioduszewski et al. 2002, in preparation) suggests some kind of explosive event. Orlandini et al. (2000) suggest a thermonuclear runaway on the surface of a white dwarf is responsible, but this seems hard to reconcile with the high inferred X-ray luminosity (Robinson et al. 2002) and the γ-ray detection by *CGRO*/BATSE (Belloni et al. 1999). It seems more likely that the outburst involved a brief burst of supercritical accretion onto a neutron star or black hole, resulting in ejection of much of the accreted material. This accounts for the observed radio ejecta and possibly the broad components of the hydrogen and helium lines. A supercritical accretion model could also involve a large enough optical depth of scattering material around the X-ray source to smear out any short timescale variability.

One possible cause for such a large burst of accretion would be the passage of the compact object through the equatorial plane. We can attempt to estimate the accretion rate, although this will be very uncertain as the orbital parameters are unknown and the physical conditions in sgB[e] star outflows are not well understood. We assume stellar parameters typical of hot, luminous sgB[e] stars (Zickgraf et al. 1986) and adopt a representative 30 year orbit of a 10 $M_\odot$ black hole around a 60 $M_\odot$ sgB[e] star with an eccentricity of $e \sim 0.9$. The periastron distance is then about 10–20 R_{star} and the periastron velocity 170 km s^{-1}. In the model of Oudmaijer et al. (1998) for HD 87643, the equatorial density at 10 R_{star} is ~2.5 × 10^{-12} g cm^{-3}. This model may not be correct, and CI Cam is probably more massive and luminous than HD 87643, but this at least indicates the kind of equatorial density which is considered plausible. The velocity of the compact object relative to the equatorial material will be dominated by its orbital motion, so the Bondi accretion rate is then predicted to be ~6 × 10^{21} g s^{-1} or ~400 $\dot{M}_{Edd}$ (Bondi 1952). Given the uncertainties mentioned above, this is a very approximate estimate, and could be at least an order of magnitude off. Even allowing for this large uncertainty, the accretion rate in this scenario can therefore be expected to be extremely high, due to the high density and low velocity of the equatorial material, and hence a supercritical accretion episode is possible. In contrast, when the compact object is out of the plane the density is lower by a factor of 10^4 (in the model of Oudmaijer et al. 1998) and the relative velocity is higher, since the high latitude outflow moves much faster. The Bondi accretion rate is then expected to be much lower, ~8 × 10^{-5} $\dot{M}_{Edd}$. If the accretion efficiency remained high, $\eta \sim 0.1$, then CI Cam should still be a relatively bright X-ray source, with $L_X \sim 10^{35}$ erg s^{-1}. However, at these low accretion rates then the flow could be expected to become advective as proposed for other quiescent black hole candidates (Narayan et al. 2001 and references therein), and the accretion efficiency would then be lower, $\eta \sim 10^{-2}$–10^{-4}, implying $L_X \sim 10^{32}$–10^{34} erg s^{-1} as observed (Robinson et al. 2002). This model therefore avoids the problem that Robinson et al. (2002) had, that a compact object burrowing through a dense spherical outflow should be persistently bright.

The passage of a compact object through the equatorial material, and the ejection of a lot of material from near it could affect the equatorial region significantly, so changes in the line spectrum from this region would be expected. We cannot offer an exact mechanism for this, however, and several factors

may be involved: the tidal effect of the compact object passage; X-ray heating; and the interaction of the expanding radio remnant with the equatorial flow. The rapid response of the lines to the outburst, peaking within a few days of the X-rays, constrains the tidal effect, as a tidally triggered disc outburst would be expected to proceed on a viscous timescale, if the disc is Keplerian (i.e. thin and rotationally supported, with small inflow or outflow velocity). This is likely to be very long, hundreds to thousands of days. It is far from clear that sgB[e] discs are Keplerian, but other timescales, e.g. the outflow time from the stellar surface to ~50 stellar radii, are likely to be similar. The extended decay of the iron lines may indeed be due to a recovery of the disc to its pre-outburst state on this timescale, but the rise of the outburst cannot be, so a tidally triggered disc outburst is unlikely.

The X-ray heating effect will obviously be much faster, and should rise and fade on a timescale comparable to the X-ray outburst itself, although could be prolonged by significant cooling or recombination times. This is not seen, although a signature of X-ray heating of the disc may be present in the form of strong 6–7 keV line emission seen by *SAX* (Frontera et al. 1998), *ASCA* (Ueda et al. 1998) and *RXTE* (Revnivtsev et al. 1999; Belloni et al. 1999). If this line is attributed to fluorescent iron emission then a large, cold, optically thick surface is needed covering about half the sky as seen from the X-ray source (Ueda et al. 1998). This is what would be expected if the X-ray source were above the plane of the equatorial material. The dramatic enhancement of high excitation lines, such as He II and N III during outburst also suggests that X-ray or extreme-UV irradiation may place a role.

The expansion of the radio ejecta can more naturally produce the timescales observed than either a tidal interaction or X-ray irradiation can. Assuming an expansion at ~5000 km s^{-1} (from Mioduszewski et al. in preparation, assuming $d \sim 5$ kpc), this would reach a disc radius of ~50 stellar radii (~2000 $R_\odot$) in about 3 days, so this is consistent with the relatively short outburst and the rise time of the Fe II *EW*s. The expanding ejecta may also explain the broad blue-shifted component seen prominently in hydrogen and helium profiles during outburst, as the inferred expansion velocities are comparable to the maximum detectable velocities in the emission lines. This is an appealing interpretation, as the origin of these ejecta is most likely the compact object, and hence an overall blue shift can be explained as the orbital velocity of the compact object at the time of ejection. The overall blue-shift seen, 50–100 km s^{-1}, is reasonable compared to our estimate of the periastron velocity ~170 km s^{-1}. It is also sensible that we see a blue-shift, rather than red, as X-ray spectra taken in the outburst decay show a strong fluorescent iron line, consistent with reflection from the equatorial material, and do not show strong absorption; both indicate that the compact object was likely between us and the equatorial plane at the time, and hence should have been moving toward us.

9.3. The origin of the optical continuum

The dramatic increase in the optical luminosity of CI Cam during the outburst is also intriguing. The optical rise was not observed, but if it was later than the X-rays then the rise time was fast, $\lesssim 2$ days. While large optical brightening is typical of SXTs, it is actually rather surprising in a system containing a hot, luminous sgB[e] star. The brightening is such that whatever provides the additional source of light during outburst must significantly outshine the sgB[e] star itself. Relative to the mean pre-outburst level (Bergner et al. 1995) the brightest magnitudes reported are brighter by 1.9 mag (U, Apr 3.9; Hynes et al. 1998), 2.1 mag (B, Apr 3.1; Garcia et al. 1998), 2.3 mag (V, Apr 3.1; Garcia et al. 1998), 3.5 mag (R, Apr 2.1; Robinson et al. 1998), 2.4 mag(I, Apr 3.8; Clark et al. 2000). These observations are not simultaneous and are not intended to indicate the spectrum; merely to indicate that the outburst was dramatic throughout the optical region. Since the peak of the outburst was missed in the optical these are actually lower limits on the outburst amplitude. While some of the brightening is due to stronger line emission, not all can be; removing the line emission from our early spectra only increases B and V by ~0.6 mag, so much of the brightening has to be enhanced continuum. Figure 4 indicates that on 1998 April 3, the excess continuum was 2–5× brighter than the sgB[e] star, and redder than it. Where can this extra continuum come from? Some possibilities which we discuss below are:

1. Heating of the sgB[e] star during the outburst.
2. Heating of the dusty envelope around the system.
3. Emission from an accretion disc around the compact object.
4. Enhanced emission from the circumstellar material around the sgB[e] star.
5. Emission related to the observed radio ejection.

To help constrain the possibilities it is useful to examine the spectrum of the excess light. Figure 15 shows the difference between the early outburst and post-outburst spectra from Fig. 4. Close examination of the outburst spectrum, and comparison with high resolution spectra taken later in outburst, indicates that although much of the spectrum is dominated by emission lines, the lowest points do appear to indicate the continuum. The difference spectrum is obviously rather uncertain, but many possibilities can be ruled out. If it is a power-law, then it is relatively flat in f_ν. The power-law model plotted is $f_\nu \propto \nu^{1/2}$. A completely flat spectrum would also be possible, but it could not be much redder or bluer than these possibilities. A hot black body is ruled out, as indicated by the fact that the difference spectrum is redder than the sgB[e] spectrum. A 10 000 K black body is shown; a temperature much cooler than this would also not be consistent with the data. Similar conclusions can be drawn by examining the change in $B - V$ during the outburst, from ~0.8 mag to $\lesssim 1.2$ mag. It is obviously difficult to be precise given the uncertain reddening and large line contribution, but a very hot or very cold black body, or a very red or very blue power-law can be ruled out.

This colour information can immediately be used to constrain the origin of the excess light. Interpretation 1 can be ruled out as heating of the sgB[e] star could not make the spectrum redder even if a 5× increase in brightness were possible. In this case, the excess should be extremely blue. Equally, interpretation 2 can be ruled out as the excess light is not cool enough.
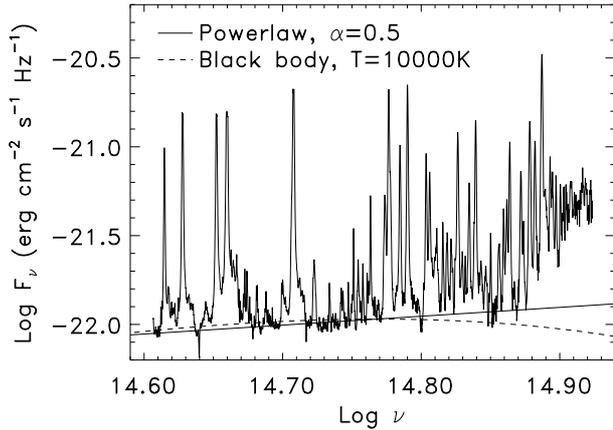
Fig. 15. Spectrum of the extra light seen in outburst, obtained by taking the difference between spectra obtained on 1998 April 3 and 1998 October 29. This has been dereddened using the Fitzpatrick (1999) extinction curve assuming $A_V = 4.0$. Two possible models for the continuum spectrum are also plotted; the power law corresponds to $F_\nu \propto \nu^{1/2}$.

Heated dust would dissociate for $T \gtrsim 2000\,\mathrm{K}$, but the observed spectrum and change in $B - V$ are clearly not consistent with such a low temperature.

The brightness of the outburst argues against interpretation 3. After correcting for line emission ($\Delta V \sim 0.6\,\mathrm{mag}$) and extinction ($A_V \sim 4\,\mathrm{mag}$), the peak dereddened continuum magnitude is $V \lesssim 5.8$ and the average quiescent value is $\langle V \rangle \sim 7.7\,\mathrm{mag}$; hence the additional continuum source has $V \lesssim 6.0$. At a distance of ~5 kpc this corresponds to an absolute magnitude of $M_V \lesssim -7.5$. This is much brighter than any low mass X-ray binary (LMXB) ($-5 < M_V < +5$; van Paradijs 1994), i.e. much brighter than other observed accretion discs around black holes or neutron stars. If the additional light were an accretion disc it would then have to be more luminous than those in LMXBs. Since the spectrum indicates that it is not extremely hot, it would have to be large. As the size of LMXB accretion discs is limited by tidal truncation, a much larger disc in CI Cam is certainly possible. If the density in the disc were comparable to the disc densities in LMXBs, however, such a large disc would provide enough mass to sustain a much longer X-ray outburst than seen, and a decay timescale of months, more like that seen in SXTs, would be expected. Indeed Robinson et al. (2002) have argued that the very rapid decay timescale in CI Cam indicates that the accretion disc, if present, must be very small. This is a very different environment from that in an LMXB, however, and the disc could be stabilised against thermal instability by irradiation from the supergiant at much lower densities than required in an LMXB, resulting in a lower disc mass. The brightness remains a problem, however, as the disc luminosity would be comparable to that of the supergiant and greater than that of the X-ray source at the same time, and so reprocessing of light from either is unlikely to dominate. It therefore seems unlikely that an accretion disc around the compact object can dominate the optical brightening in outburst.

The relatively low temperature and large area inferred for the excess light, if it originates in black body emission,

can more plausibly be associated with the equatorial material around the sgB[e] star than an accretion disc around the compact object. For a temperature of ~10 000 K, the extra emission requires an area ~40× that of the sgB[e] star. Both the temperature and size are plausible for the equatorial material around a sgB[e] star. In this case the timescale arguments are similar to those for the lines. The optical decay appears slower than the X-rays (e.g. Clark et al. 2000). The peak optical luminosity of the continuum source is also large; for $T \sim 10\,000\,\mathrm{K}$ and an area ~40× that of the star, the luminosity was at least $\sim 2 \times 10^5\,L_\odot \sim 8 \times 10^{38}\,\mathrm{erg\,s^{-1}}$ (assuming $d \sim 5\,\mathrm{kpc}$). This is actually larger than the peak X-ray luminosity at this distance, $L_X \sim 3 \times 10^{38}\,\mathrm{erg\,s^{-1}}$, and by the time of the optical observations, the X-ray flux had already dropped by more than an order of magnitude (Belloni et al. 1999). Both the decay timescale and optical luminosity render it unlikely that the continuum brightening can come from X-ray reprocessing. The timescales would be more plausible for an interaction of the equatorial material with the radio ejecta; assuming an expansion speed ~5000 km s⁻¹, this area will be covered in less than half a day, so a rapid optical brightening is possible in this way, i.e. powered by the kinetic energy of the ejecta.

The remaining possibility is that there is a considerable direct optical contribution from the ejecta from the explosion. The similarity of timescales of the optical and radio decay (Clark et al. 2000) argue for this interpretation. Optical synchrotron can probably be ruled out. The dereddened magnitude of the additional continuum component of $V \lesssim 6$ corresponds to a flux of $\gtrsim 15\,\mathrm{Jy}$ early in the outburst. Contemporaneous radio observations were much weaker than this, with the spectral energy distribution peaking at 650 mJy at 8.4 GHz and decreasing at higher frequencies (Hjellming & Mioduszewski 1998b). Optical synchrotron emission thus seems unlikely without a very unusual electron energy distribution. However, if the accretion rate was highly supercritical, we might expect much of the energy released to be reprocessed by a scattering envelope to produce a bright optical source (Shakura & Sunyaev 1973). Such a supercritical accretion scenario has been invoked for a number of X-ray binaries. SS 433 is likely to a persistently supercritical source (e.g. Fabrika 1997 and other authors; see also Okuda & Fujita 2000 and references therein). V4641 Sgr, which also had an extremely short but luminous X-ray outburst has been suggested to have undergone a transient burst of supercritical accretion (Revnivtsev et al. 2002). Shakura & Sunyaev (1973) predict that the optical spectrum in the supercritical regime should appear as a power-law, $F_\nu \propto \nu^{1/2}$, saturated with broad emission lines. We have already discussed the origin of the broad emission lines that we see and suggested that these may be related to outflowing material from supercritical accretion. The outburst optical continuum emission is clearly redder than the underlying star, and the excess continuum emission is consistent with a $F_\nu \propto \nu^{1/2}$ power law (Fig. 15). This therefore does seem a plausible interpretation. If this supercritical accretion scenario is correct, then the observations suggest that the accretion rate was extremely high and hence the spherisation radius large; assuming a terminal velocity for the ejected material of ~5000 km s⁻¹, and an optical luminosity ~10³⁸ erg s⁻¹,

suggests an accretion rate of $\dot{M} \sim 10^2$–$10^4\,\dot{M}_{\mathrm{crit}}$ (Shakura & Sunyaev 1973), consistent with our estimate above of the possible periastron accretion rate.

All of these calculations are extremely simplistic. Our aim is not to present a detailed spectral model, but rather to test which explanations of the outburst emission are plausible. X-ray heating, whether of the sgB[e] star itself, the equatorial material, an accretion disc around the compact object or extended dust, is not consistent with observations. Heating of the equatorial material by the interaction with the expanding radio remnant, or direct emission from these ejecta, remain possibilities. The latter has the advantage that invoking a supercritical accretion regime explains both the optical continuum emission and the broad, blue-shifted emission components, so is our favoured interpretation, but it is likely that a combination of these mechanisms is involved.

9.4. Is CI Cam an X-ray binary?

Finally we emphasise that none of the preceding discussion depends on CI Cam being a binary system. We, and others, have argued that CI Cam is an sgB[e] star, and a compact object of some kind is clearly implicated in the X-ray outburst, but it is not necessary for them to be physically associated. Indeed, the properties of CI Cam in quiescence are sufficiently similar to other hot, luminous sgB[e] stars that if it is a binary then the compact object's influence appears to only be important during an outburst. For example, it clearly does not truncate the disc as can happen in classical Be X-ray binaries. While it could be that CI Cam does have a compact object in a long period orbit, it is also possible that the outburst could have resulted from a chance encounter of an isolated black hole or neutron star with the circumstellar material. As a massive, young object, CI Cam is likely located in a region of recent star formation, so there are likely to be many stellar remnants in its proximity. While such a chance encounter still seems improbable, it cannot be disproved based on the statistics of a single event. So far we have no conclusive evidence for the binarity of CI Cam. Barsukova et al. (2002) have suggested that two periodicities are present. Their short 11.7 day period is certainly too small to represent the orbital period in a system such as this as the compact object would have to be almost on the surface of the sgB[e] star, or even inside it. The longer 1100 day period would be more plausible, but cannot be considered convincing until it is seen to repeat for multiple cycles. In balance, while the hypothesis that CI Cam is a binary seems most likely, it is not proven and the alternative, that there was a chance encounter with an isolated compact object, cannot be ruled out.

10. Summary and conclusions

CI Cam is an sgB[e] star, and many of its characteristics, particularly the emission line spectrum, are representative of this class. Comparison with other sgB[e] stars suggests that CI Cam is among the hottest members of the class and viewed nearly pole-on. It differs from the other sgB[e] stars in interacting with a compact star which introduces an additional variable element. It seems most likely that the compact object is physically associated with CI Cam, i.e. that it is an HMXB. In this case, the compact object is probably in a long period, eccentric orbit. However we cannot rule out the possibility that this was a chance encounter and that the two stars are not physically associated. Resolution of this issue will likely involve waiting for a true periodicity, repeated over several cycles, or another outburst. In considering the outburst mechanism, there is actually little difference between a long period eccentric orbit and a chance encounter, so our discussion of the outburst applies to both cases.

We suggest that the majority of the optical emission lines originate from an equatorially concentrated outflow or circumstellar disc. During outburst, hydrogen and helium lines appear to have two components, a narrow rest component and a moderately blueshifted broad component. Metallic lines are mainly dominated by the narrow component at all times, although some asymmetry is seen in outburst suggesting that a broad component is present. The square profiles of the Fe II lines can be explained by the equatorial outflow model, if viewed pole-on, so the narrow component is likely associated with this. The broad component becomes weaker and narrower on the decline, and almost disappears in quiescence. This may come from material ejected in the outburst rather than from the equatorial outflow. Forbidden lines fall into two categories; [O I] and [Fe II] show similar line profiles to Fe II, but with a lack of low velocity material. These profiles could originate from the low density, upper layers of the equatorial outflow. Other forbidden lines, [N II] and [O III] are narrower and likely come from a much more extended region.

The outburst mechanism remains undetermined, although the outburst was probably precipitated by the passage of the compact object through the equatorial material. It is unlikely that X-ray heating of any component is responsible for the optical outburst. Instead the optical outburst is likely associated with the expanding remnant produced by the X-ray outburst, either through direct emission from the remnant or as a result of its interaction with the circumstellar material. The spectral shape of the outburst optical continuum, and the presence of broad, blue-shifted emission components, are both consistent with predictions for supercritical accretion resulting in ejection of much of the material (Shakura & Sunyaev 1973), and the peak mass transfer rate for an equatorial passage of the compact object is indeed predicted to be well above the Eddington limit.

After the outburst changes in the emission lines persist for at least three years, with Fe II lines stronger than before and He I, He II, and N II lines weaker. The timescale for the extended Fe II decay, at least, is similar to the expected viscous timescale of the disc of hundreds to thousands of days, so this may indicate the gradual recovery of the disc to its equilibrium state. As the system does not yet appear to have stabilised continued monitoring is important to determine if the system eventually recovers to the pre-outburst state or if it settles to a different level.

References

Allen, D. A., & Swings, J. P. 1976, A&A, 47, 293

Barsukova, E. A., Fabrika, S. N., Pustilnik, S. A., & Ugryumov, A. V. 1998, Bull. Spec. Astrophys. Obs., 45, 147

Barsukova, E. A., Borisov, N. V., Goranskij, V. P., Lyuty, V. M., & Metlova, N. V. 2002, Astron. Rep., 46, 275

Bondi, H. 1952, MNRAS, 112, 195

Brand, J., & Blitz, L. 1993, A&A, 275, 67

Belloni, T., Dieters, S., van den Ancker, M. E., et al. 1999, ApJ, 527, 345

Bergner, Yu. K., Miroshnichenko, A. S., Yudin, R. V., et al. 1995, A&AS, 112, 221

Bjorkman, J. E. 1998, B[e] stars, ed. C. Jaschek, & A. M. Hubert (Kluwer Academic Publishers), 189

Chakrabarty, D., & Roche, P. 1997, ApJ, 489, 254

Chkhikvadze, Y. N. 1970, Astrofizika, 6, 65

Clark, J. S., Steele, I. A., Fender, R. P., & Coe, M. J. 1999, A&A, 348, 888

Clark, J. S., Miroshnichenko, A. S., Larionov, V. M., et al. 2000, A&A, 356, 50

Downes, R. A. 1984, PASP, 96, 807

Drabek, S. V., Kopylov, I. M., Somov, N. N., & Somova, T. A. 1986, Bull. Spec. Astrophys. Obs., 22, 64

Fabrika, S. N. 1997, Ap&SS, 252, 439

Fitzpatrick, E. L. 1999, PASP, 111, 63

Frontera, F., Orlandini, M., Amati, L., et al. 1998, A&A, 339, 69

Garcia, M. R., Berlind, P., Barton, E., et al. 1998, IAU Circ., 6865

Grandi, S. A. 1980, ApJ, 238, 10

Herbig, G. H. 1975, ApJ, 196, 129

Herbig, G. H. 1993, ApJ, 407, 142

Hjellming, R. M., & Mioduszewski, A. J. 1998a, IAU Circ., 6857

Hjellming, R. M., & Mioduszewski, A. J. 1998b, IAU Circ., 6862

Humphreys, R. M. 1978, ApJS, 38, 309

Hynes, R. I., Roche, P., Haswell, C. A., et al. 1998, IAU Circ., 6871

Ikeda, Y., Kawabata, K. S., & Akitaya, H. 2000, A&A, 355, 256

Jaschek, C., & Andrillat, Y. 2000, in The Be Phenomenon in Early-Type Stars, IAU Coll., 175, ed. M. A. Smith, H. F. Henrichs, & J. Fabregat, ASP Conf. Ser., 214

Krelowski, J., Walker, G. A. H., Grieve, G. R., & Hill, G. M. 1987, ApJ, 316, 449

Kupka, F., Piskunov, N., Ryabchikova, T. A., Stempels, H. C., & Weiss, W. W. 1999, A&AS, 138, 119

Lamers, H. J. G. L. M., Zickgraf, F.-J., de Winter, D., Houziaux, L., & Zorec, J. 1998, A&A, 340, 117

McClintock, J. E., Canizares, C. R., & Tarter, C. B. 1975, ApJ, 198, 641

Marshall, F. E., Strohmayer, T. E., Lewin, W. H. G., et al. 1998, IAU Circ., 6857

Merrill, P. W., & Burwell, C. G. 1933, ApJ, 78, 87

Miroshnichenko, A. S. 1995, Astron. & Astrophys. Trans., 6, 251

Miroshnichenko, A. S. 1996, A&A, 312, 941

Munari, U., & Zwitter, T. 1997, A&A, 318, 269

Narayan, R., Garcia, M. R., & McClintock, J. E. 2001, to appear in Proc. IX Marcel Grossmann Meet., ed. V. Gurzadyan, R. Jantzen, & R. Ruffini (World Scientific, Singapore) [astro-ph/0107387]

Okazaki, A. T. 2001, PASJ, 53, 119

Okuda, T., & Fujita, M. 2000, PASJ, 52, L5

Olling, R. F., & Merrifield, M. R. 1998, MNRAS, 297, 943

Orlandini, M., Parmar, A. N., Frontera, F., et al. 2000, A&A, 356, 163

Orr, A., Parmar, A. N., Orlandini M., et al. 1998, A&A, 340, L19

Osterbrock, D. E. 1989, Astrophysics of Gaseous Nebulae and Active Galactic Nuclei (University Science Books, Mill Valley, California)

Oudmaijer, R. D., Proga, D., Drew, J. E., & de Winter, D. 1998, MNRAS, 300, 1700

Revnivtsev, M., Emelyanov, A., & Borozdin, K. 1999, Astr. Lett., 25, 294

Revnivtsev, M., Sunyaev, R., Gilfanov, M., & Churazov, E. 2002, A&A, 385, 904

Robinson, E. L., Welsh, W. F., Adams, M. T., & Cornell, M. E. 1998, IAU Circ., 6862

Robinson, E. L., Ivans, I. I., & Welsh, W. F. 2002, ApJ, 565, 1169

Shakura, N. I., & Sunyaev, R. A. 1973, A&A, 24, 337

Smith, D., Remillard, R., Swank, J., & Smith, E. 1998, IAU Circ., 6855

Stellingwerf, R. F. 1978, ApJ, 224, 953

Traub, W. A., Millan-Gabet, R. S., & Garcia, M. R. 1998, BAAS, 30, 1330

Ueda, Y., Ishida, M., Inoue, H., et al. 1998, ApJ, 508, L167

van Paradijs, J., & McClintock, J. E. 1994, A&A, 290, 133

Wagner, R. M., & Starrfield, S. G. 1998, IAU Circ., 6857

Walborn, N. R., Parker, J. Wm., & Nichols, J. S. 1995, IUE Atlas of B-type Spectra from 1200 to 1900 Å, NASA Ref. Pub., 1363

Wood, K., Brown, J. C., & Fox, G. F. 1993, A&A, 271, 492

Zickgraf, F.-J., Wolf, B., Stahl, O., Leitherer, C., & Klare, G. 1985, A&A, 143, 421

Zickgraf, F.-J., Wolf, B., Stahl, O., Leitherer, C., & Appenzeller, I. 1986, A&A, 163, 119

Zorec, J. 1998, in B[e] Stars, ed. A. M. Hubert, & C. Jaschek (Kluwer, Dordrecht), 1